Freeform Lens Fabrication (3D printing)

Zhihan Hong OPTI-521 presentation

November, 2016

Outline

- Introduction (application, commercial, advantage)
- Printing/Freeform design
- Lens building technology
  - Fabrication
    - Diamond turning machine
    - Surface cutting polishing
    - Molding
  - Printing
  - Velocity mapping image
- Limitation
- Conclusion

Freeform design

(www.asphericon.com)

- Aspheric lens
- Axicon
- Acylinder
- Parabolic mirror

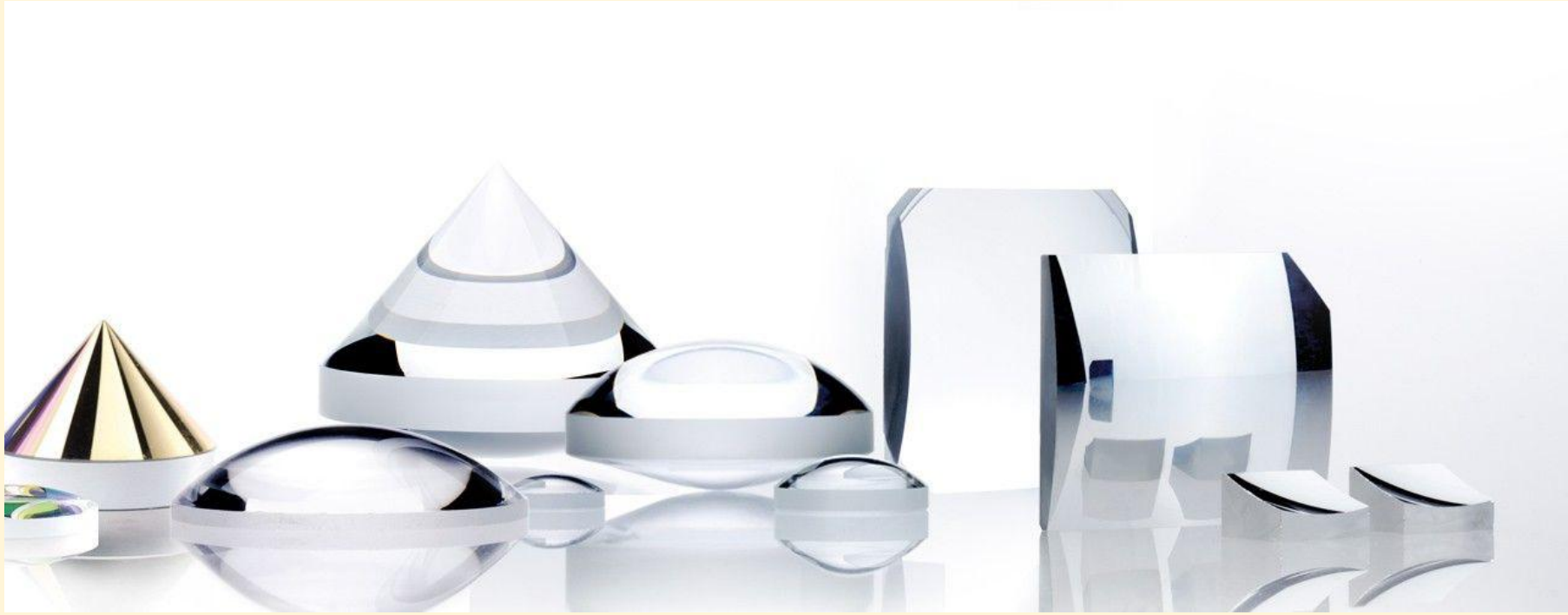

nanoscribe (www.nanoscribe.com)

- NIR laser source
- Microstructure
- Life science

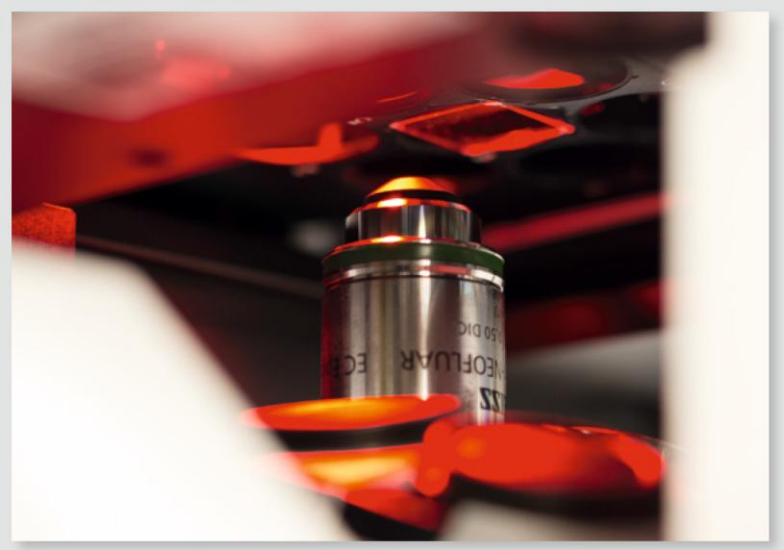

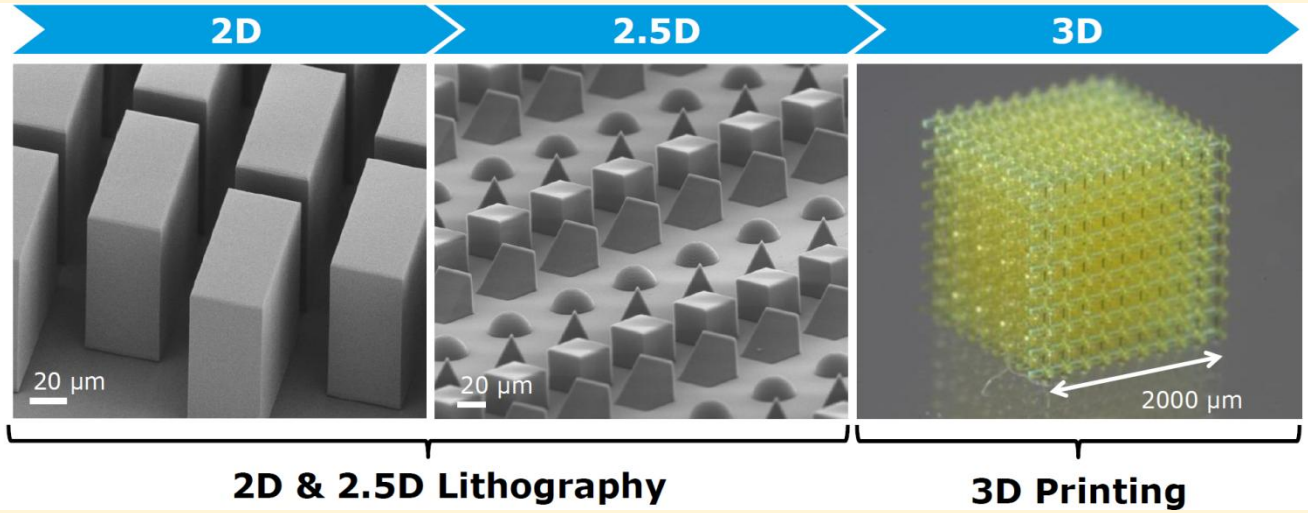

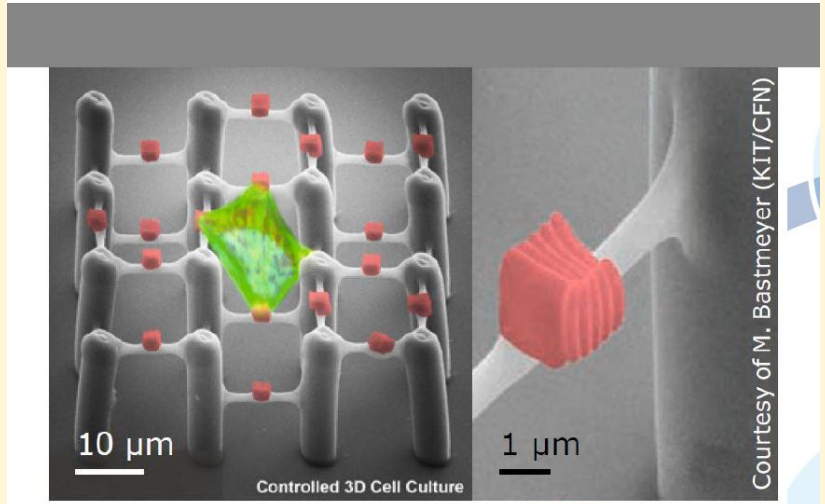

Fabrication of customized cell adhesive / cell repellent scaffolds

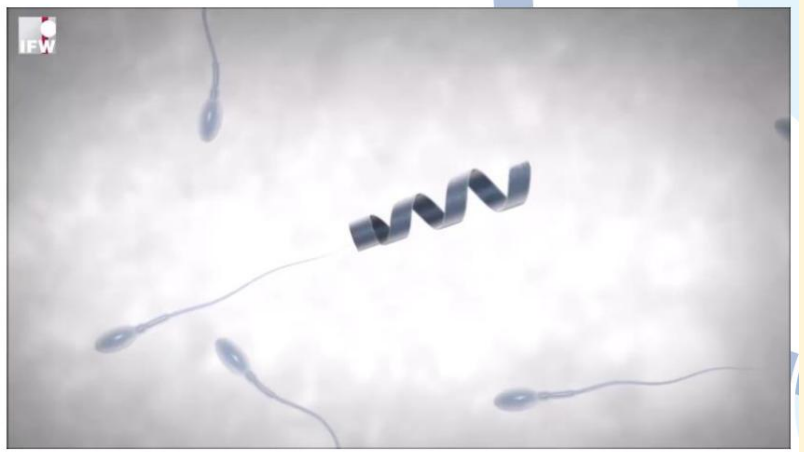

Hydrogel cargo-loaded microrobots for minimal invasive intervention

(www.luxexcel.com)

- UV laser source
- Lighting
- Automotive
- Aerospace
- Eyewear
- Drop method

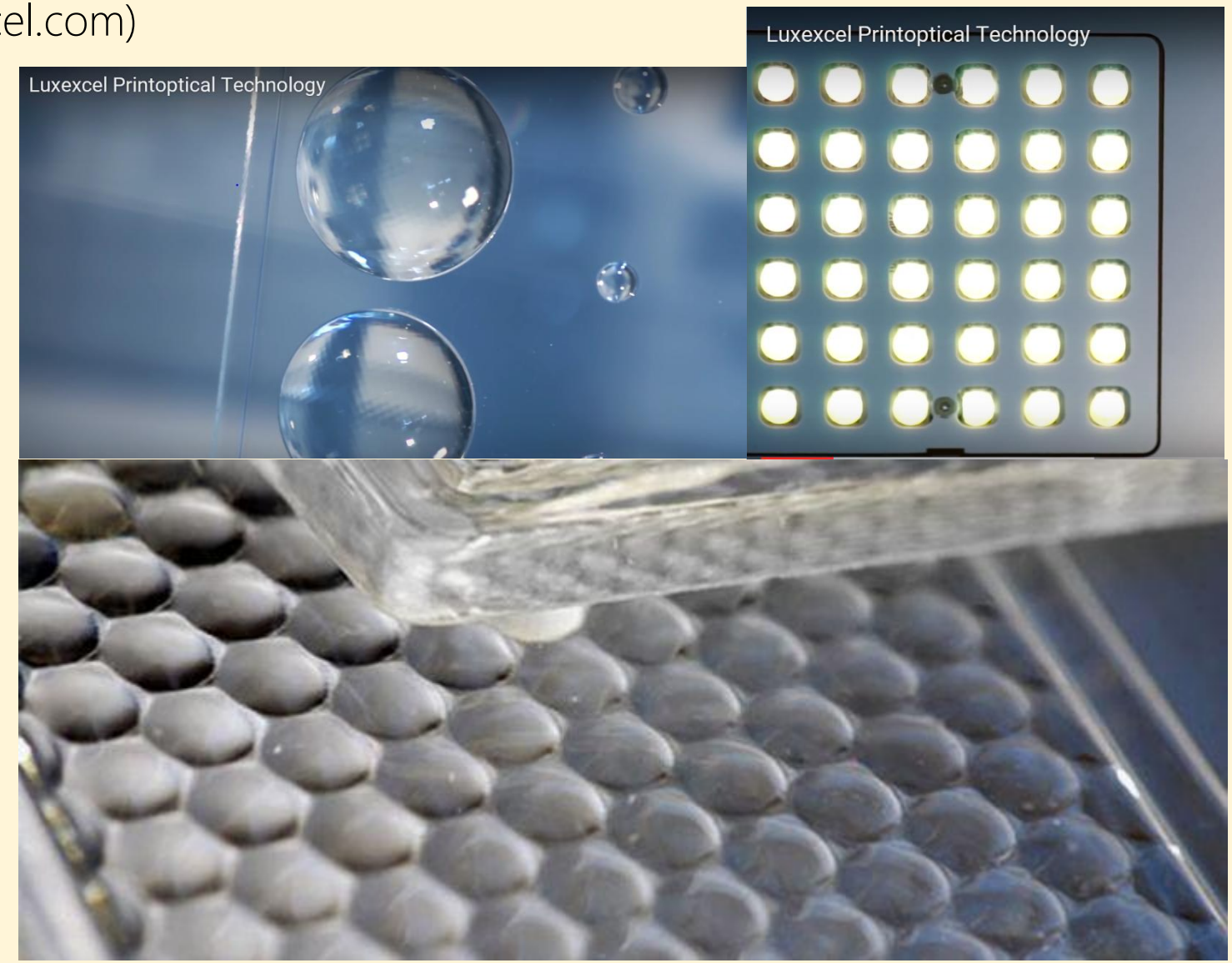

Donglin Ma. " Exploration of Ray Mapping Methodology in Freeform Optics Design for Non-Imaging Applications" .

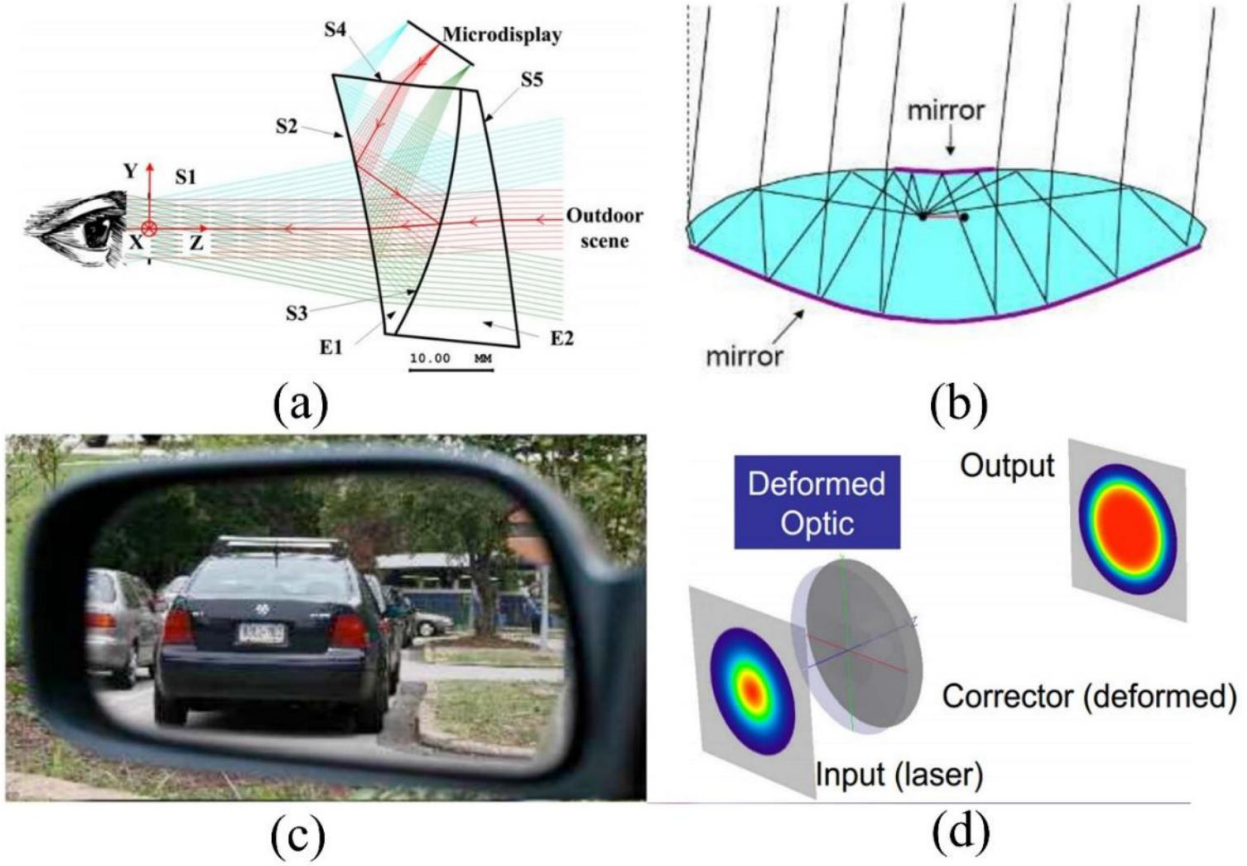

Figure 1.2 Typical applications of freeform optics: (a) freeform prism eyepiece for head-mounted display; (b) solar concentrator; (c) rear-view mirror with no blind-spot; (d) laser beam shaper. [41-44]

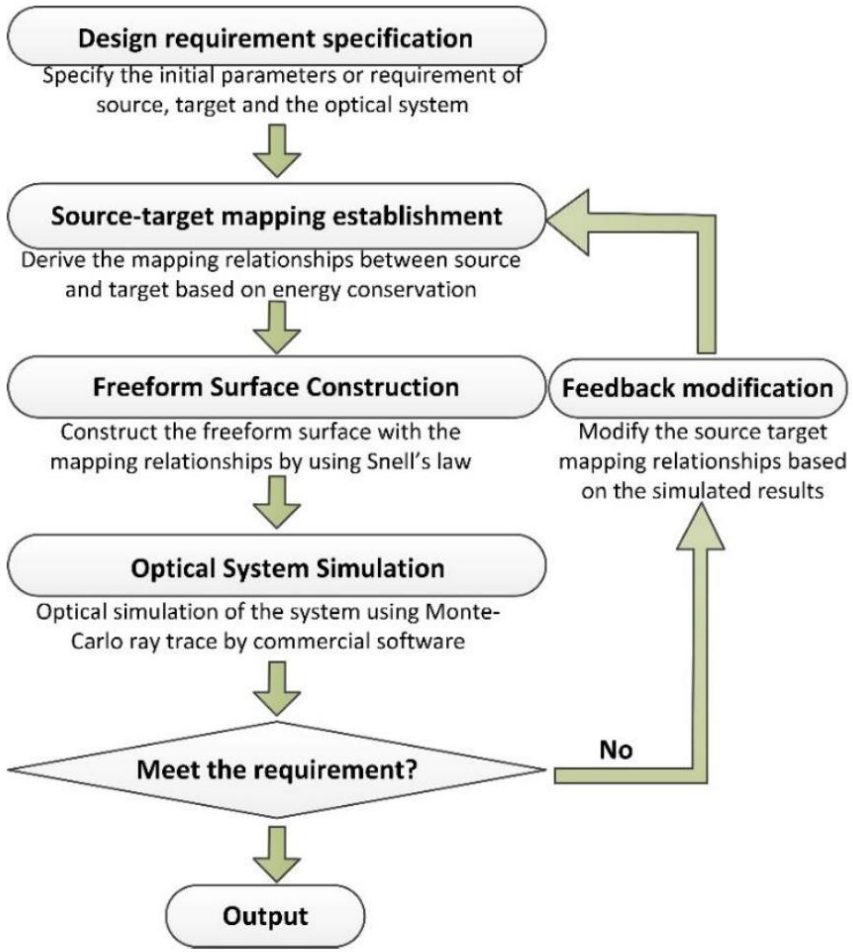

Figure 2.2 Flow diagram of the design process [68]

Donglin Ma. " Exploration of Ray Mapping Methodology in Freeform Optics Design for Non-Imaging Applications" .

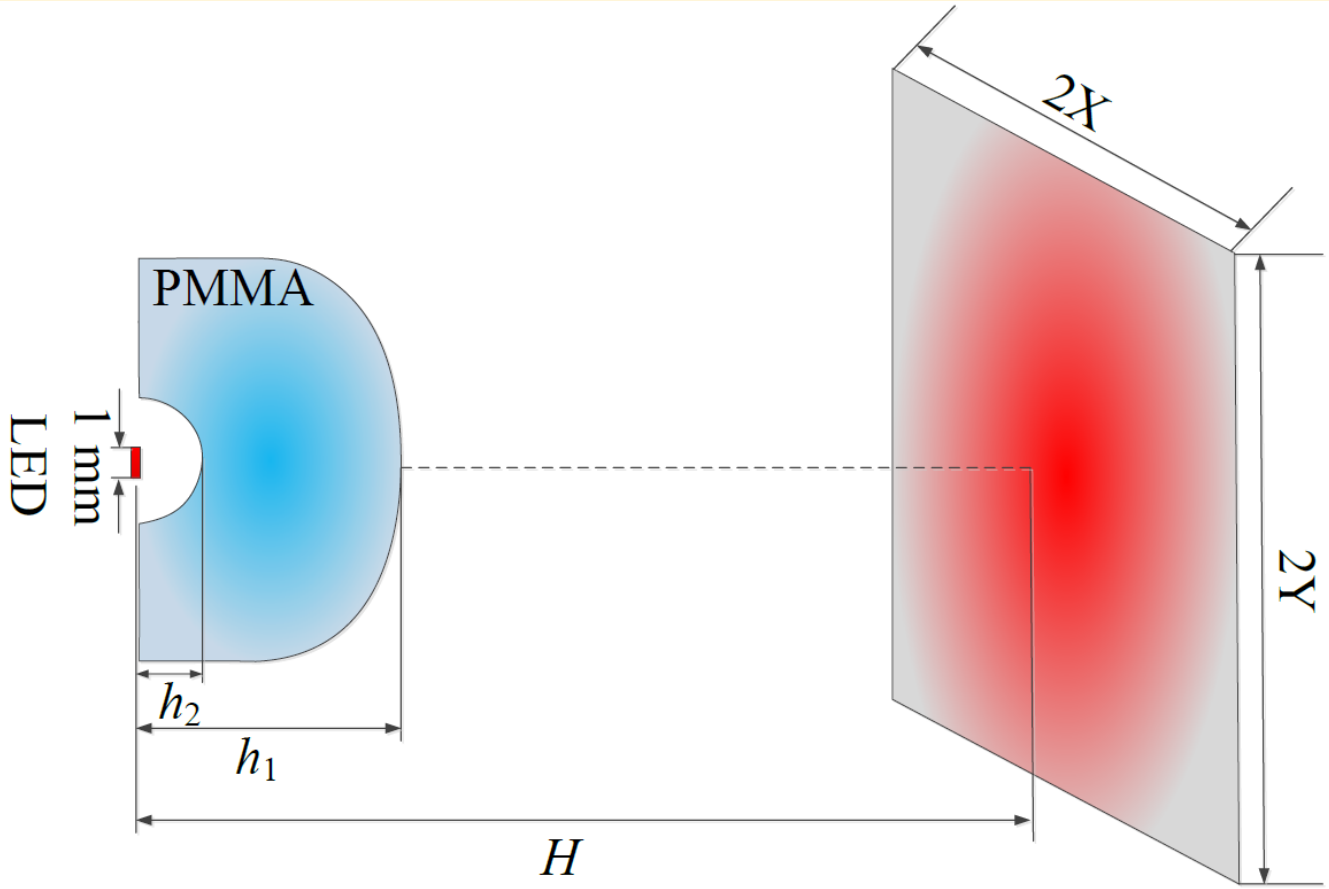

Figure 2.1 Design parameters

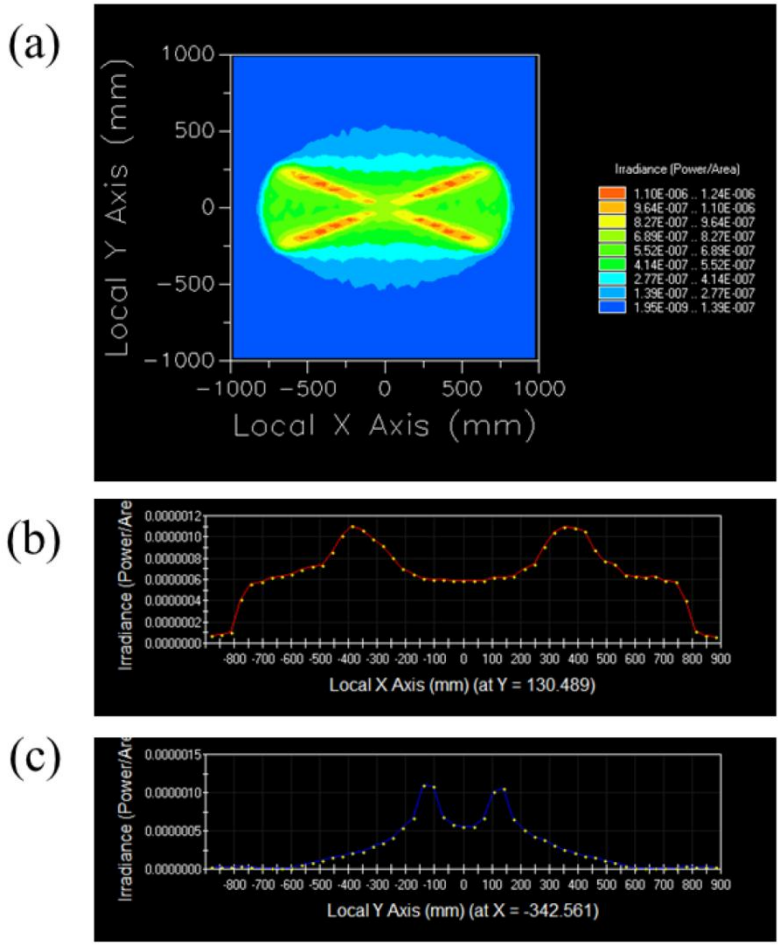

Figure 2.7 Simulation results for θ-φ ray mapping: (a) irradiance distribution; (b) x profile; (c) y profile.

Donglin Ma. " Exploration of Ray Mapping Methodology in Freeform Optics Design for Non-Imaging Applications" .

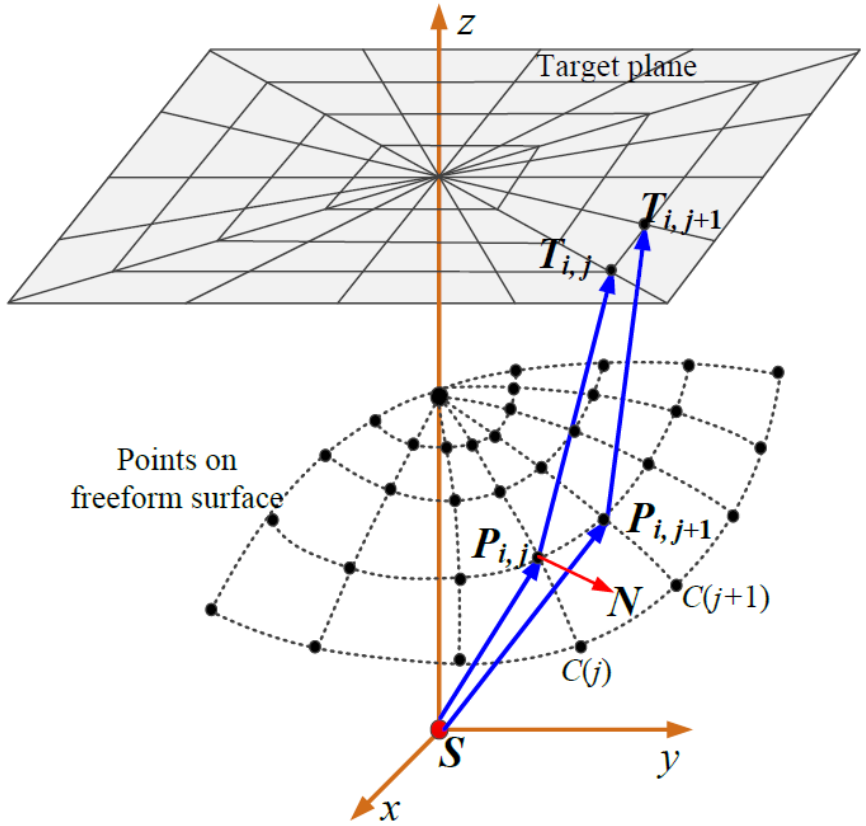

Figure 2.5 Diagram for freeform surface construction in (θ, φ) coordinate system

$$[1+n^2-2n(\boldsymbol{Out}\cdot\boldsymbol{In})]^{1/2}\cdot\boldsymbol{N}=\boldsymbol{Out}-n\cdot\boldsymbol{In}, \tag{2.11}$$

where ***In***, ***Out*** are the unit incident vector and unit output vector separately, and they can be expressed by

$$\boldsymbol{In}=\overrightarrow{\boldsymbol{SP}}/\left|\overrightarrow{\boldsymbol{SP}}\right|, \tag{2.12}$$

$$\boldsymbol{Out}=\overrightarrow{\boldsymbol{PT}}/\left|\overrightarrow{\boldsymbol{PT}}\right|. \tag{2.13}$$

Now with the information of the normal vector field, we can build the whole freeform surface. The exact calculation procedures will be introduced in the next section.

normal vector field at point $P_{i,j}$ can be derived according to Equation (2.11). Assuming $P_{i,j}$ on curve $C(j)$ is a known quantity, the neighboring point $P_{i,j+1}$ on next curve $C(j+1)$ can be calculated from the following equation:

$$(\boldsymbol{P}_{i,j+1}-\boldsymbol{P}_{i,j})\bullet\boldsymbol{N}=0. \tag{2.14}$$

Donglin Ma. " Exploration of Ray Mapping Methodology in Freeform Optics Design for Non-Imaging Applications" .

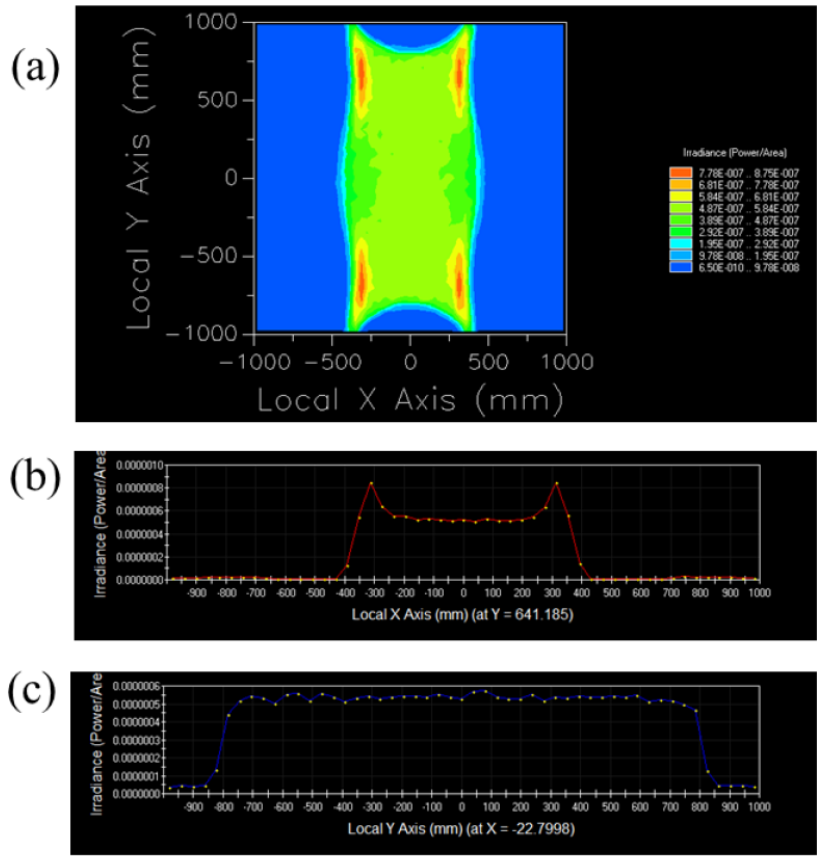

Figure 2.11. Simulation results for (*u, v*) ray mapping: (a) irradiance distribution; (b). profile; (c) *y* profile.

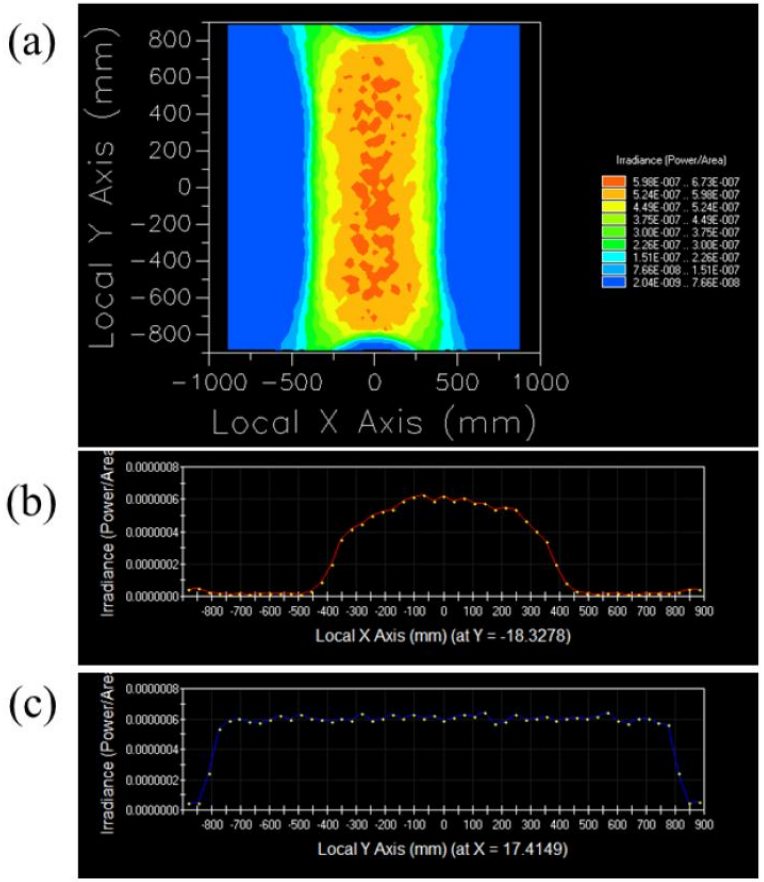

Figure 2.15 Simulation results for *u*-*v* ray mapping: (a) irradiance distribution; (b) *x* profile; (c) *y* profile.

Donglin Ma. " Exploration of Ray Mapping Methodology in Freeform Optics Design for Non-Imaging Applications" .

3.1.1 DOUBLE-POLE RAY MAPPING MECHANISM

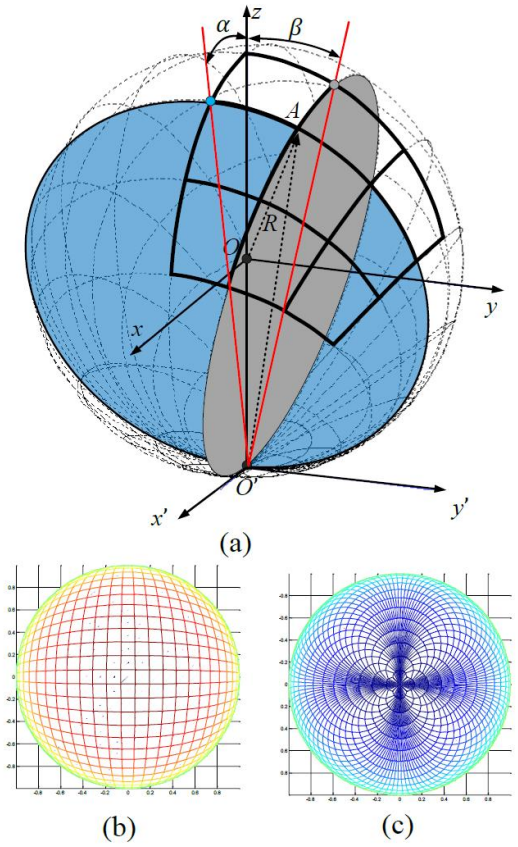

Figure 3.1 Diagram for double pole coordinate system: (a) perspective view; (b) top view; (c) bottom view.

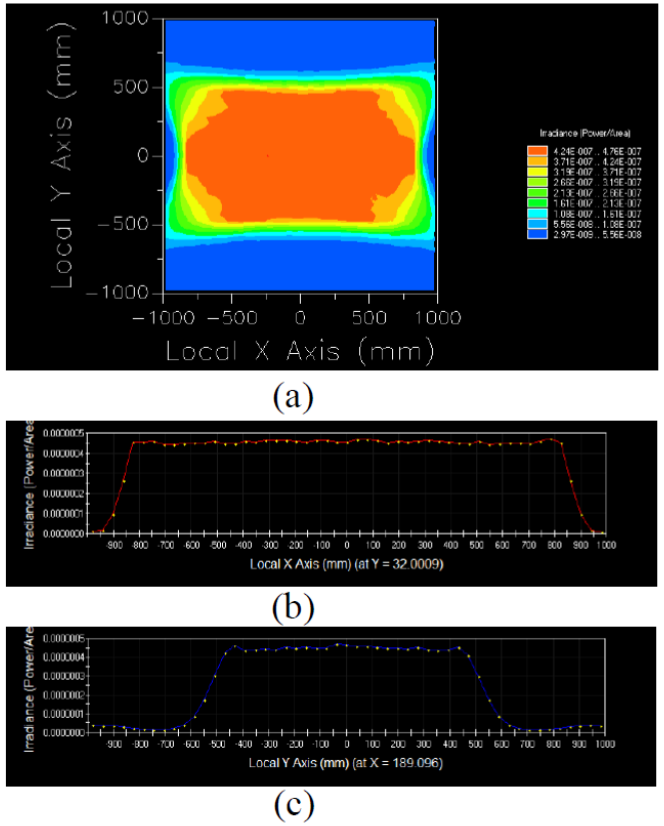

Figure 3.8 Simulation results in FRED software: (a) irradiance distribution, (b) X profile plot, and (c) Y profile plot.

Donglin Ma. " Exploration of Ray Mapping Methodology in Freeform Optics Design for Non-Imaging Applications" .

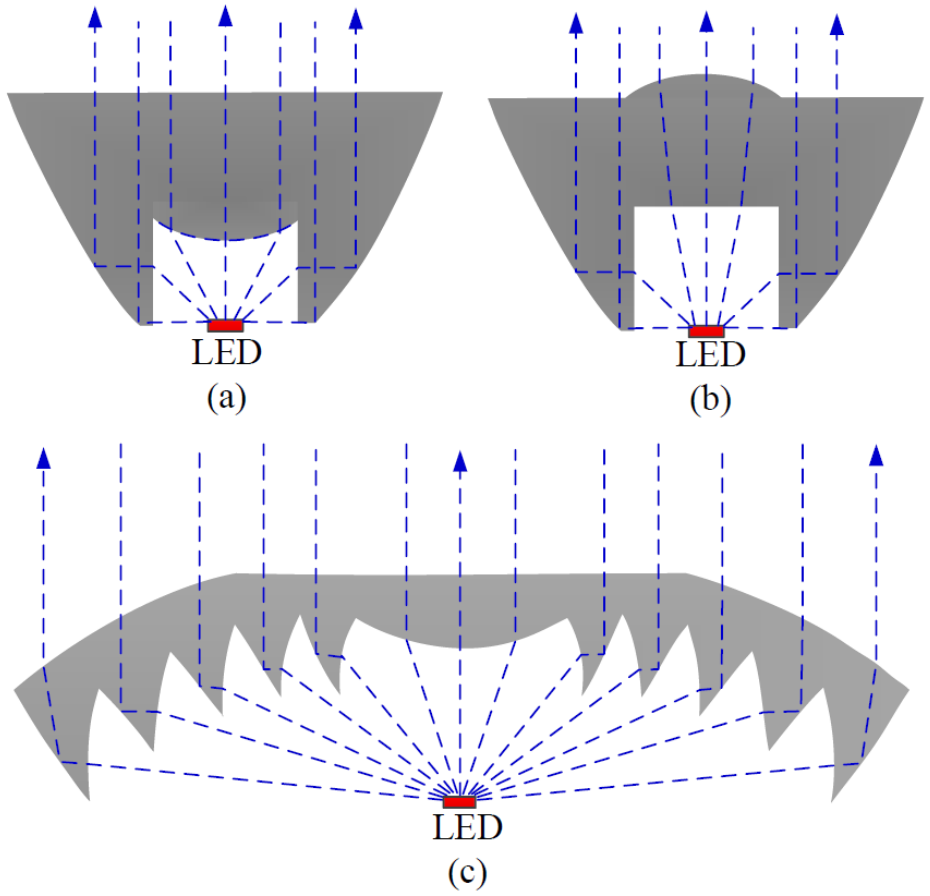

Figure 4.1 (a) TIR lens with outside flat top surface, (b) TIR lens with inside flat top surface; (c) TIR lens with faceted (Fresnel) TIR surface [88]

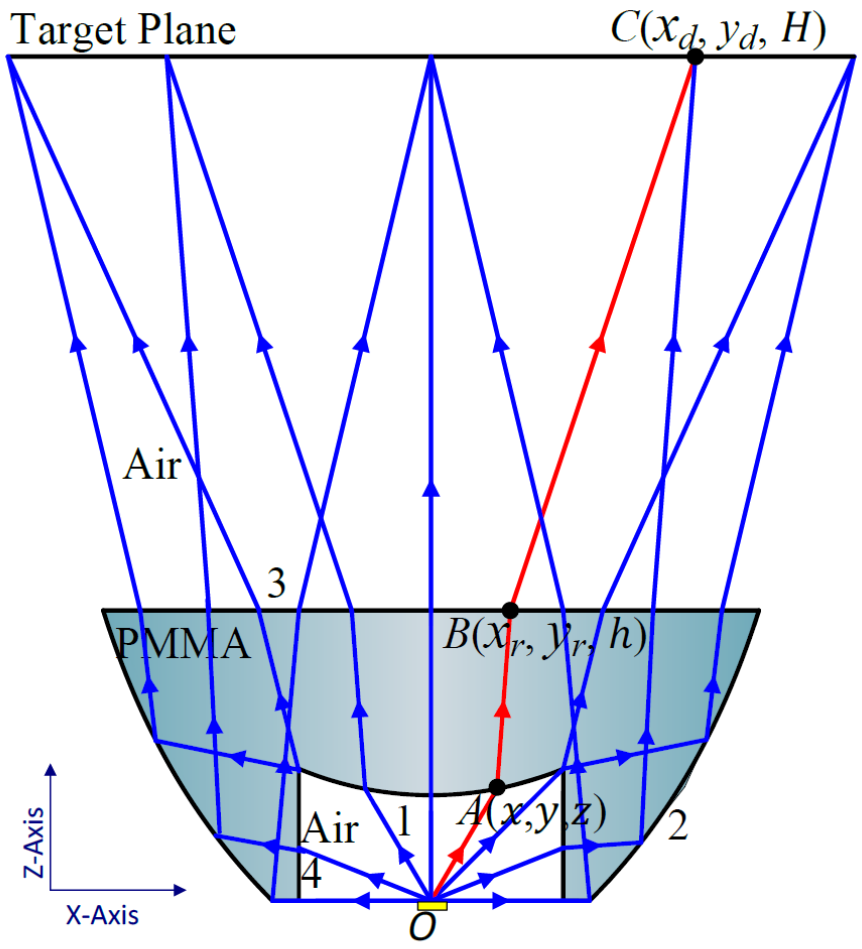

Figure 4.3 Ray trace of TIR freeform lens in 2D diagram

Qiang Liu., et al. " Long-stroke fast tool servo and a tool setting method for freeform optics fabrication." aJilin University, School of Mechanical Science and Engineering, Changchun 0086130025, China.

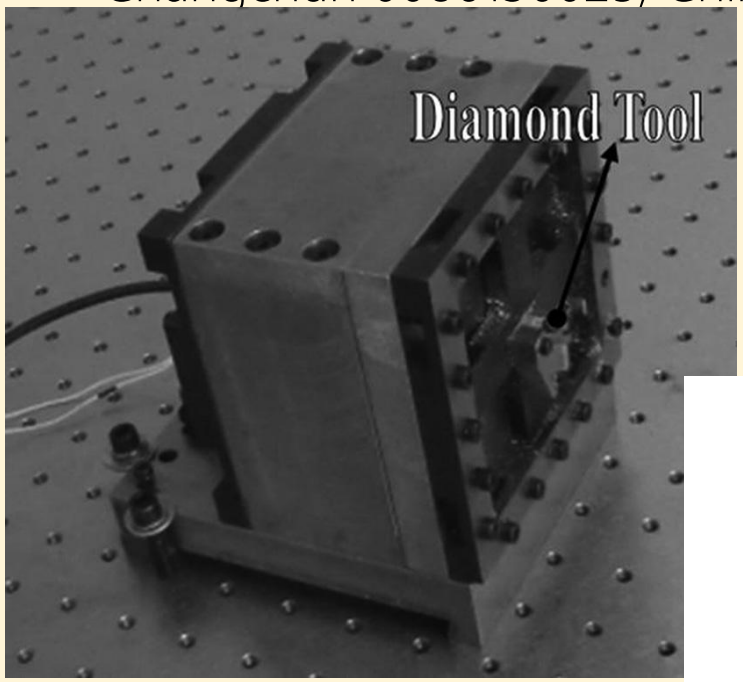

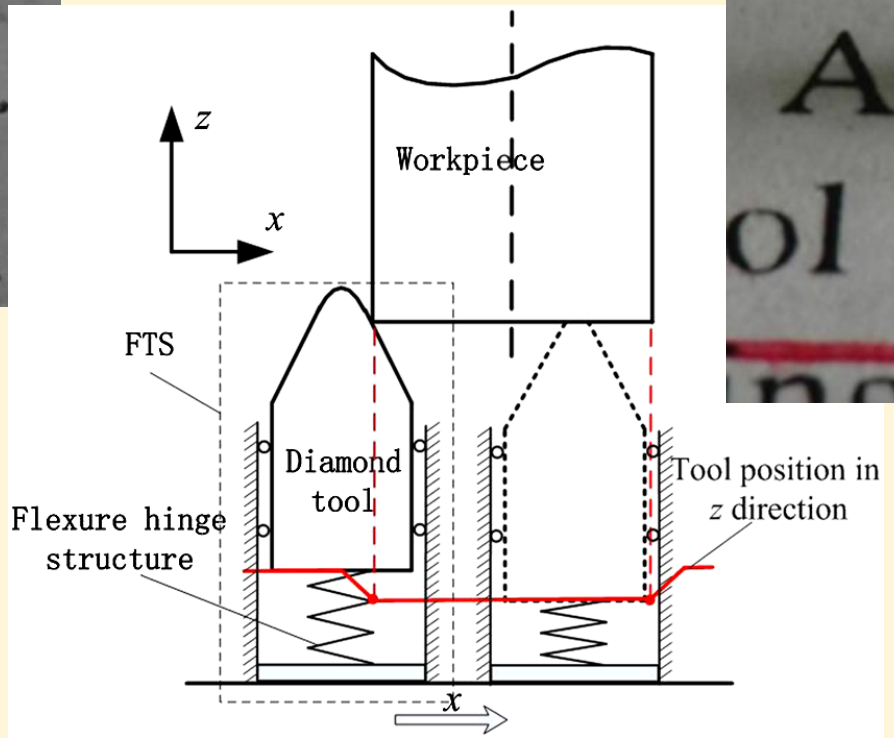

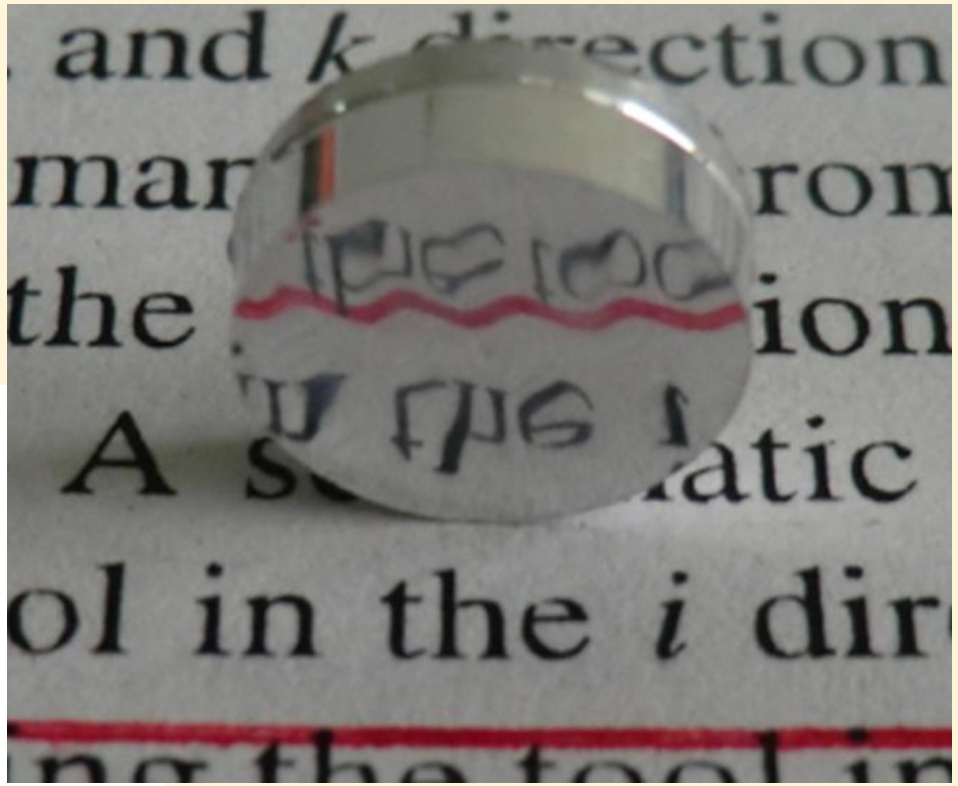

(www.iap.uni-jena.de/Applied+Computa_+tional+Optics/Seminar+schedule+.html)

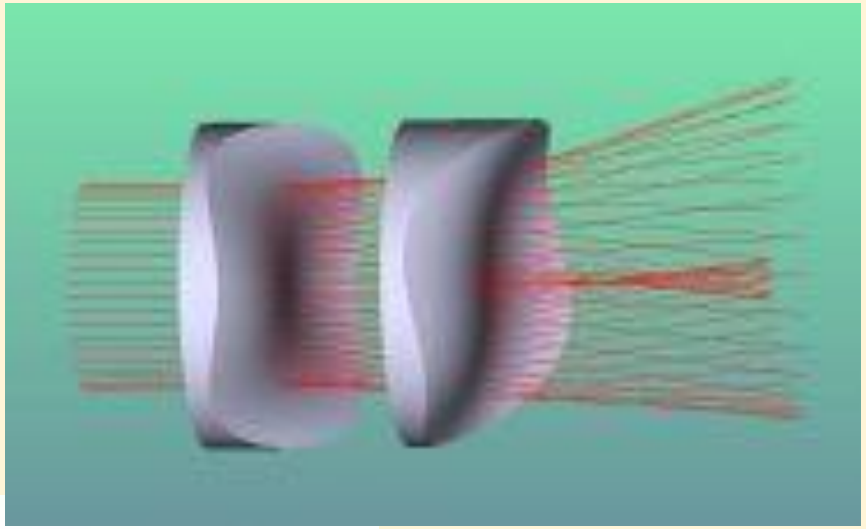

- Beam path through Alvarez lens
- Beam path through Alvarez lens

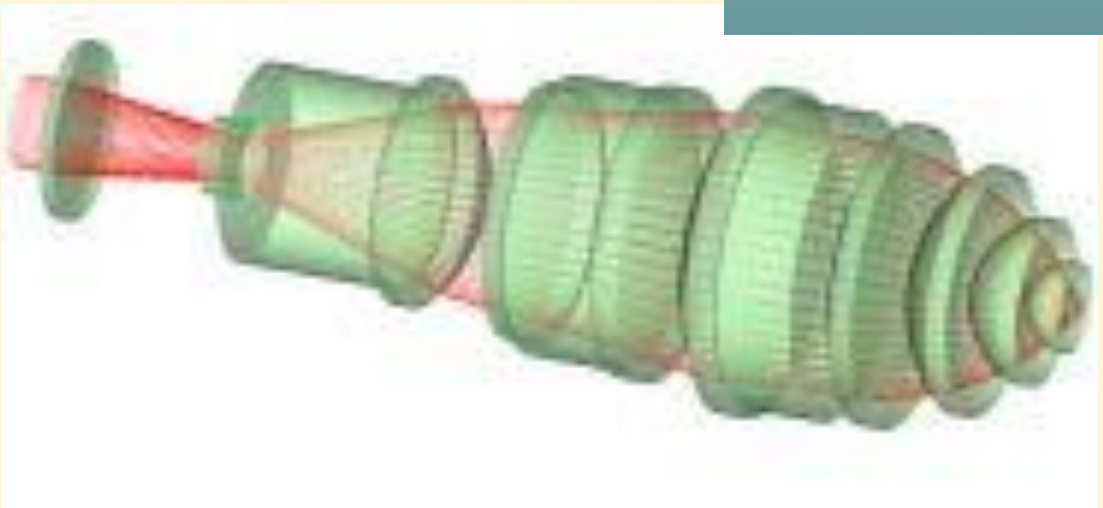

(www.asphericon.com)

- Aspheric lens
- Axicon

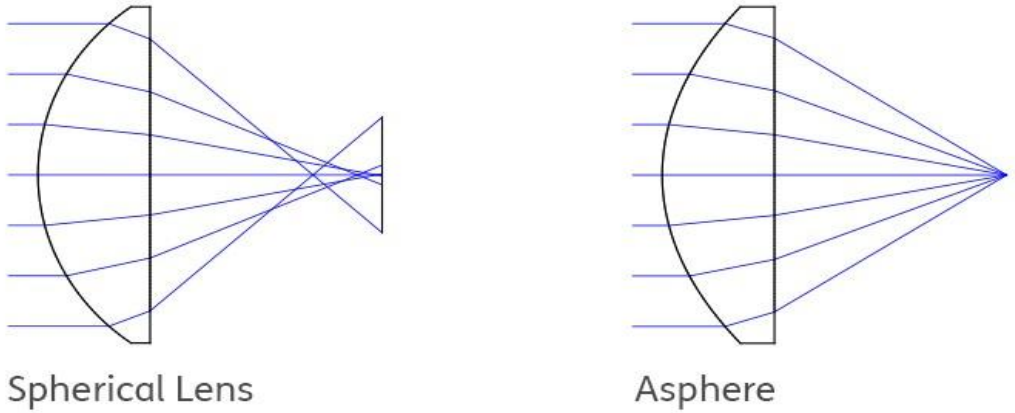

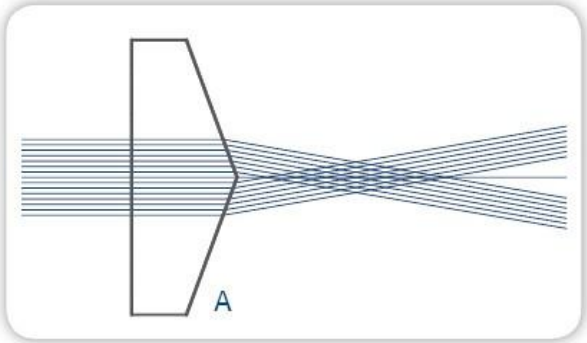

1. Generation of a Bessel beam.

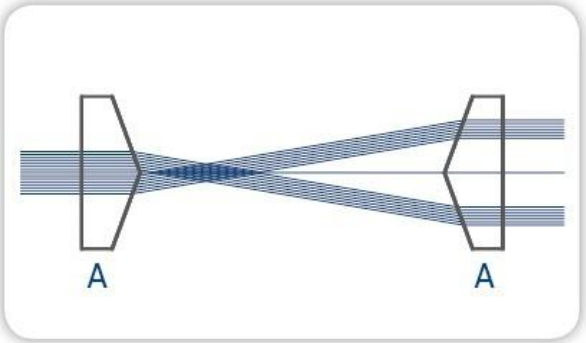

2. Generation of a ring-shaped beam.

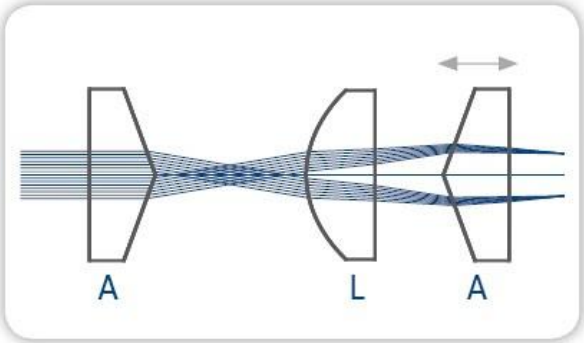

3. Generation of variable ring foci

A - Axicon | L - Lens

asphericon (www.asphericon.com)

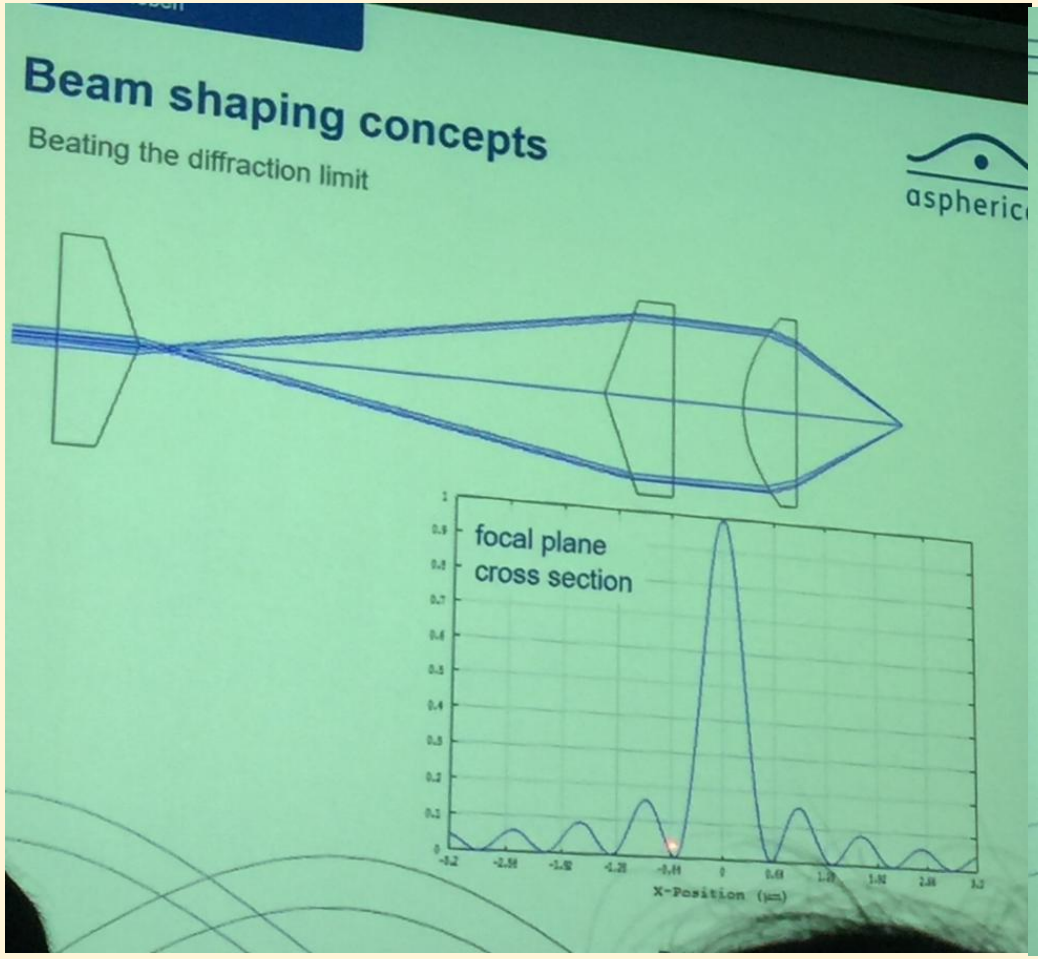

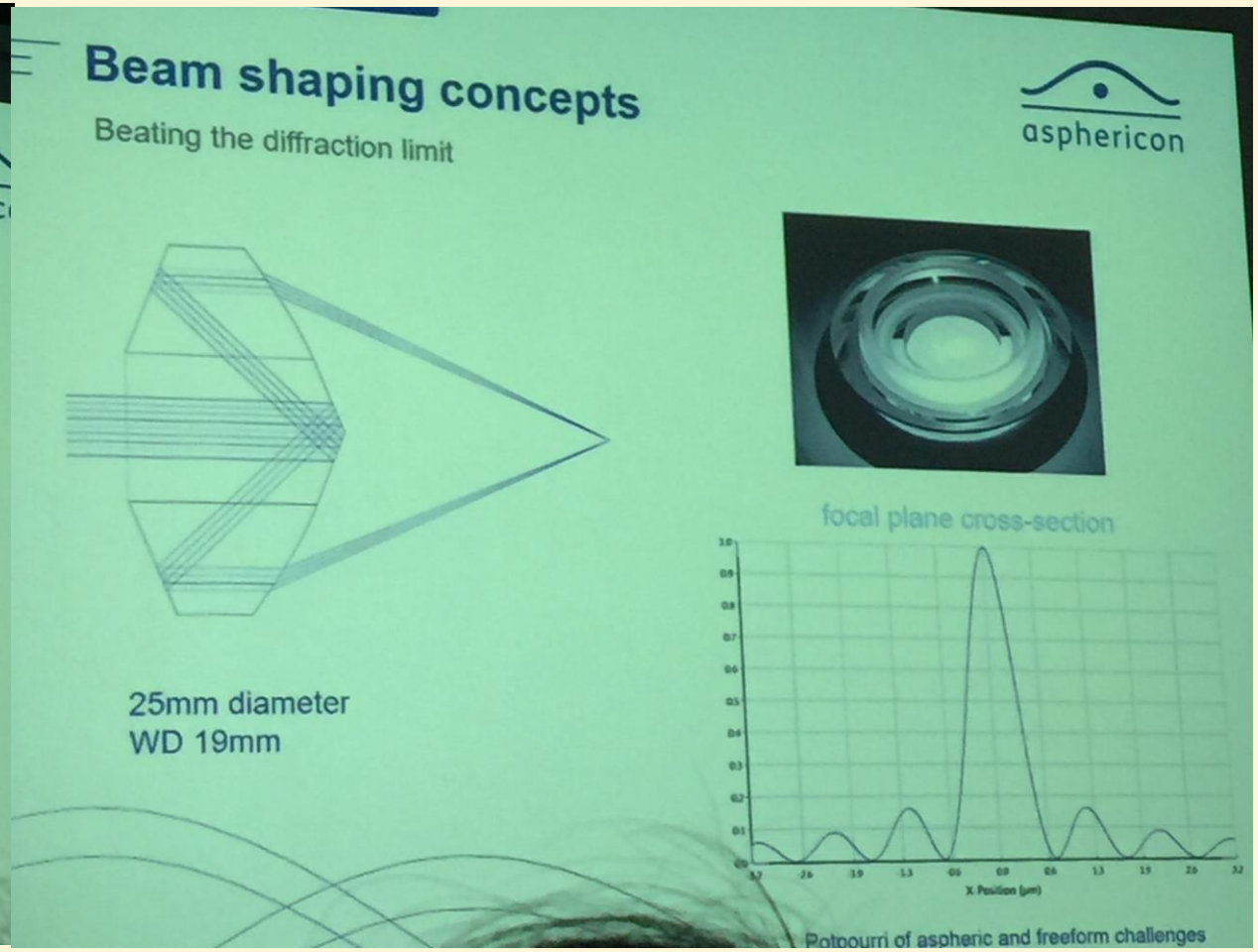

Lens building technology

Diamond turning machine

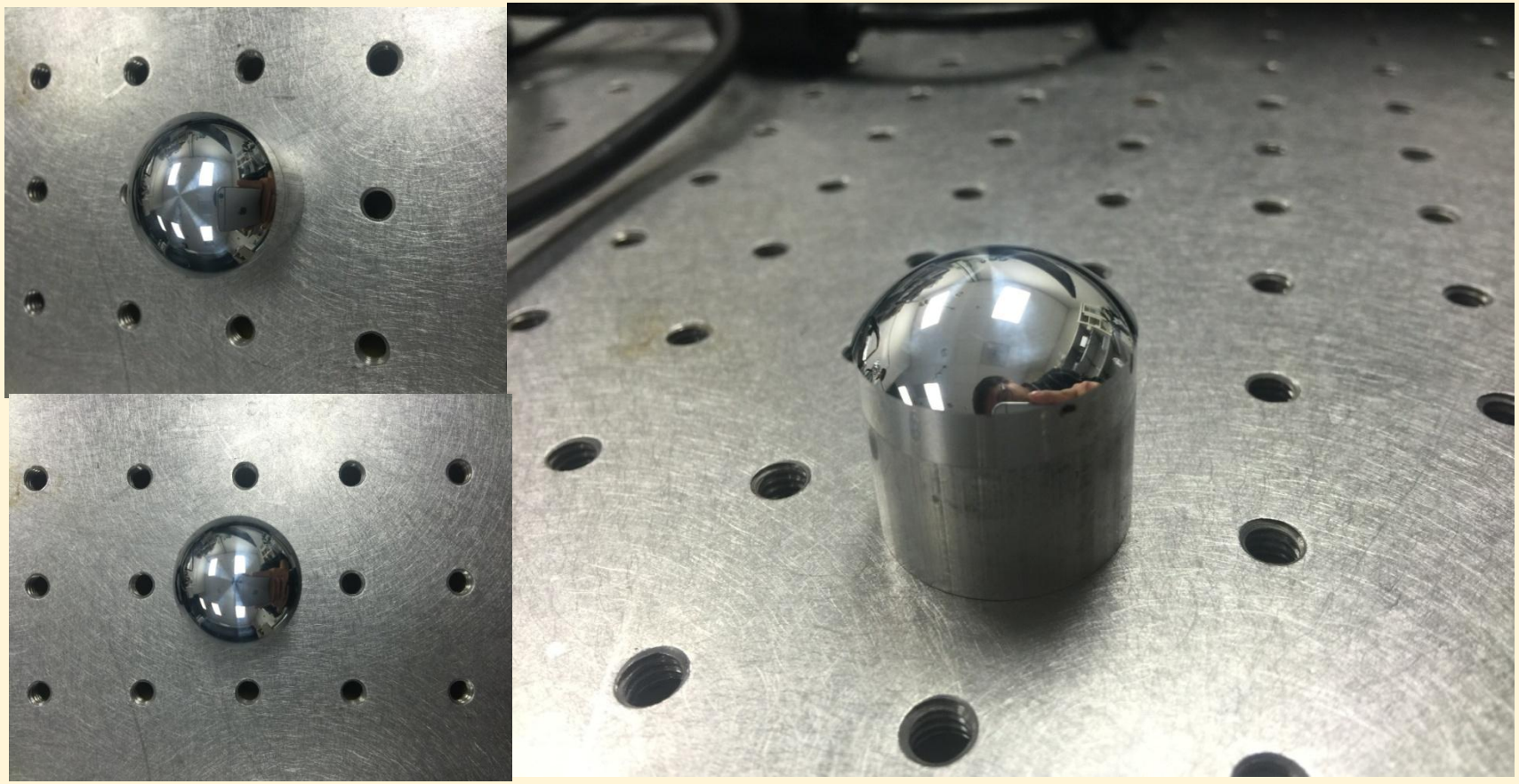

Diameter 1.00 inch Surface radius 16 mm

Diamond turning machine

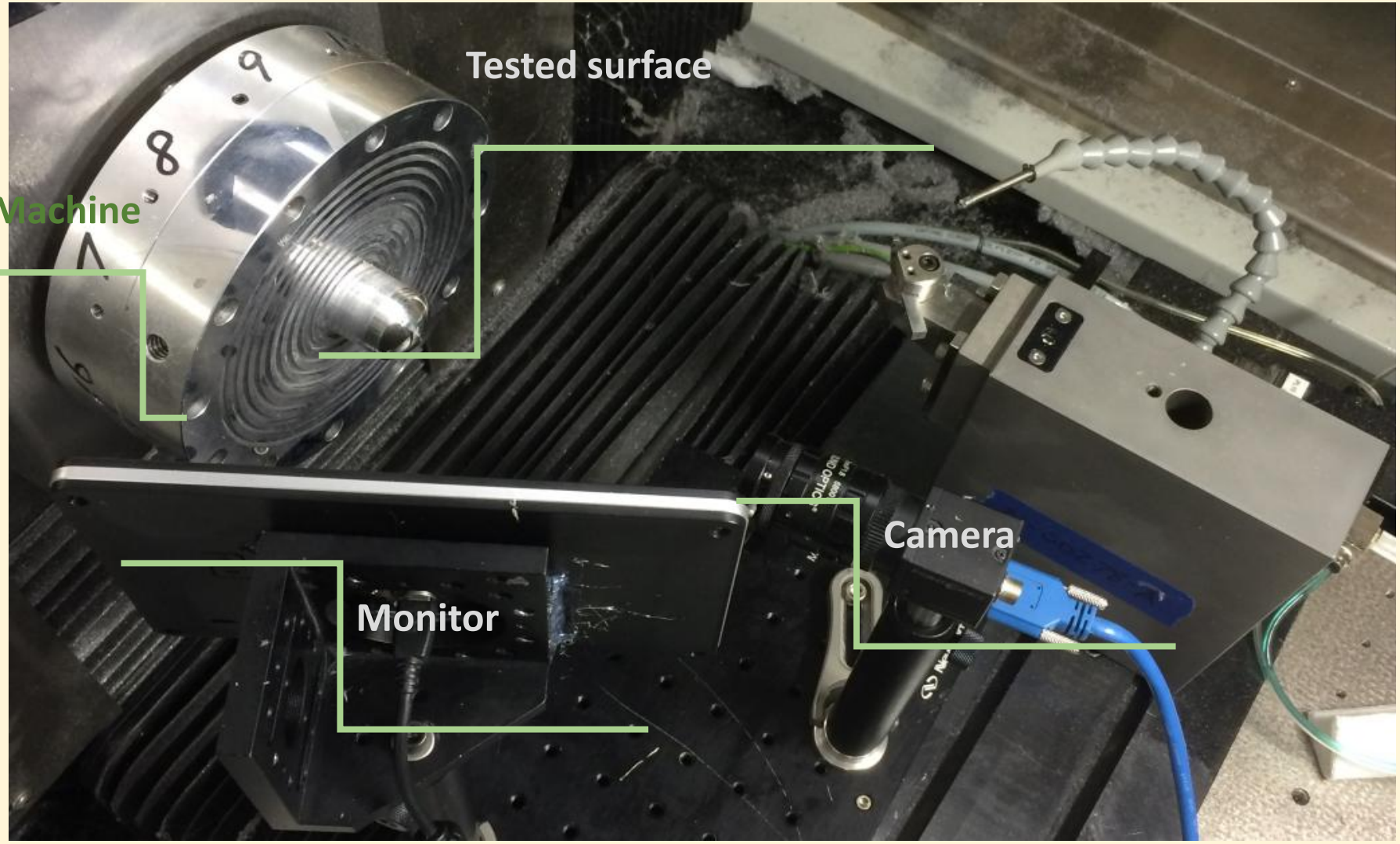

L. B. Kong, C. F. Cheung, W. B. Lee, and S. To. "An Integrated Manufacturing System for the Design, Fabrication, and Measurement of Ultra-Precision Freeform Optics." 244 IEEE TRANSACTIONS ON ELECTRONICS PACKAGING MANUFACTURING, VOL. 33, NO. 4, OCTOBER 2010.

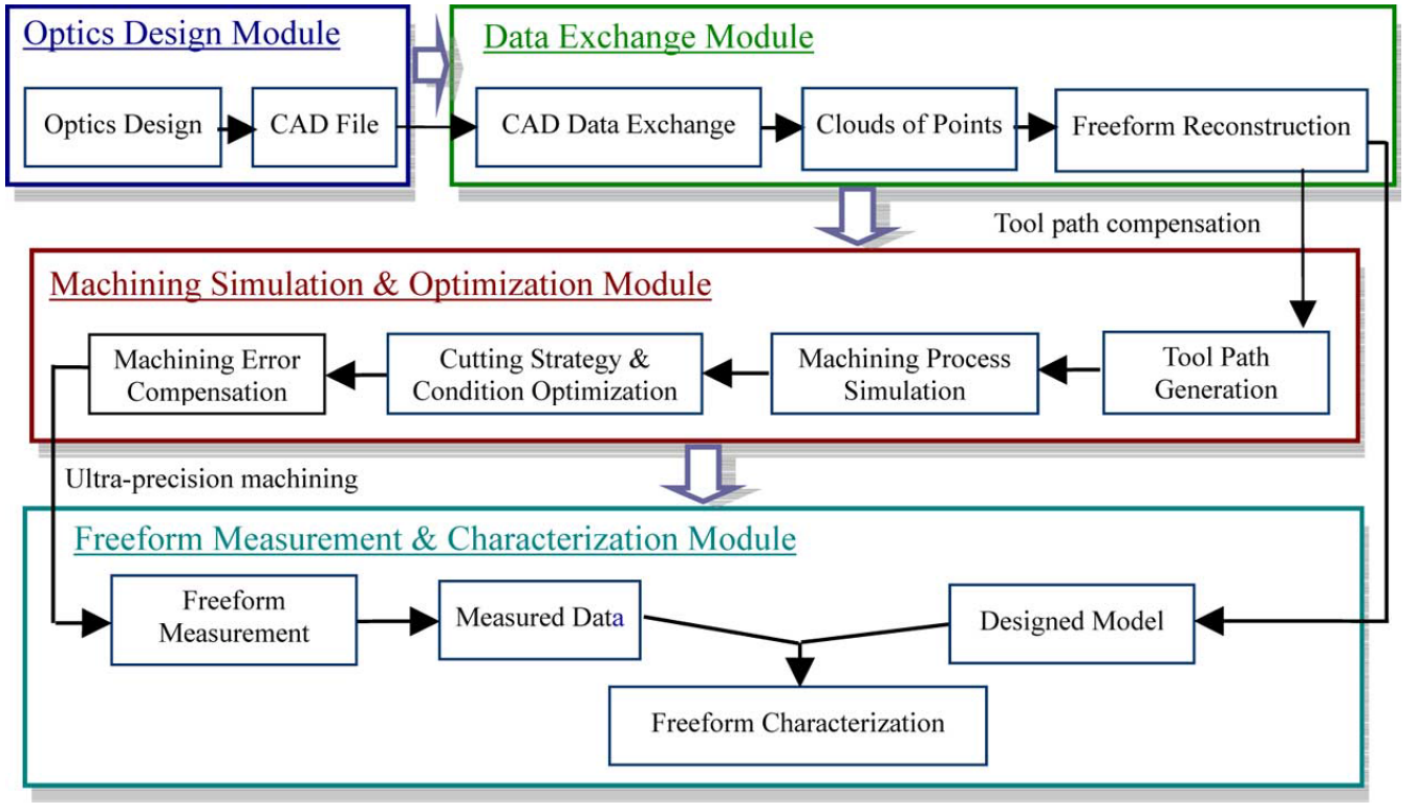

Fig. 1. Layout of the integrated system for freeform optics design, fabrication, and measurement.

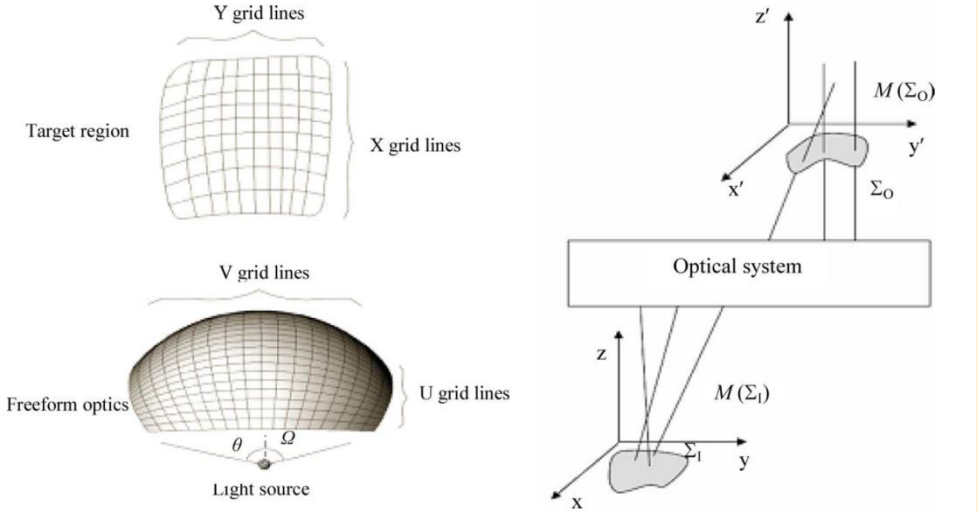

In Fig. 2, the conservation for edge-ray Etendue can be expressed as

$$E\left[M(\Sigma_O)\right] = E[M(\Sigma_I)] = n^2 \int\int dA \cos\theta d\Omega \qquad (1)$$

L. B. Kong, C. F. Cheung, W. B. Lee, and S. To. "An Integrated Manufacturing System for the Design, Fabrication, and Measurement of Ultra-Precision Freeform Optics." 244 IEEE TRANSACTIONS ON ELECTRONICS PACKAGING MANUFACTURING, VOL. 33, NO. 4, OCTOBER 2010.

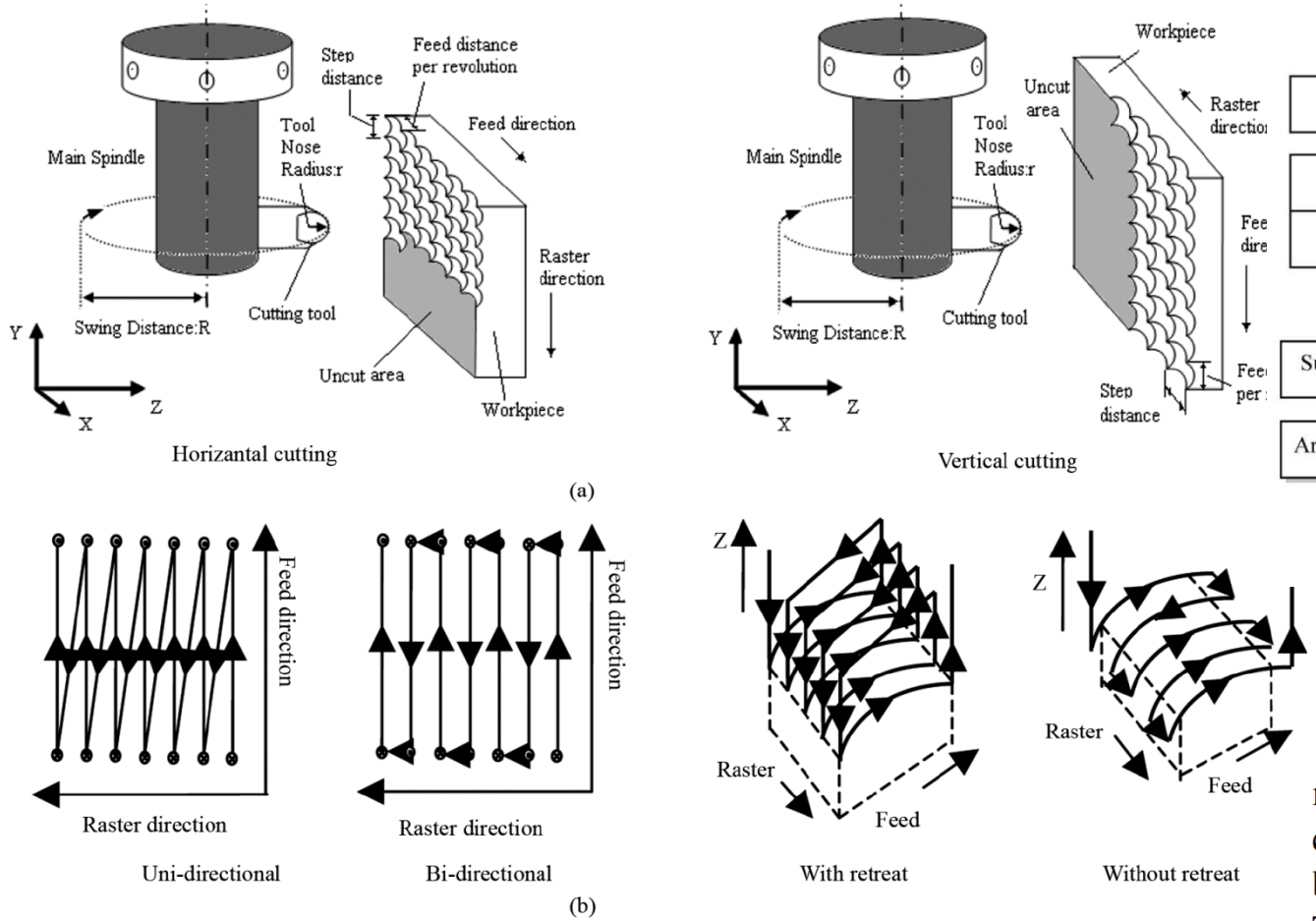

Fig. 4. Machining strategies for ultra-precision raster milling. (a) Cutting Strategies. (b) Cutting path planning.

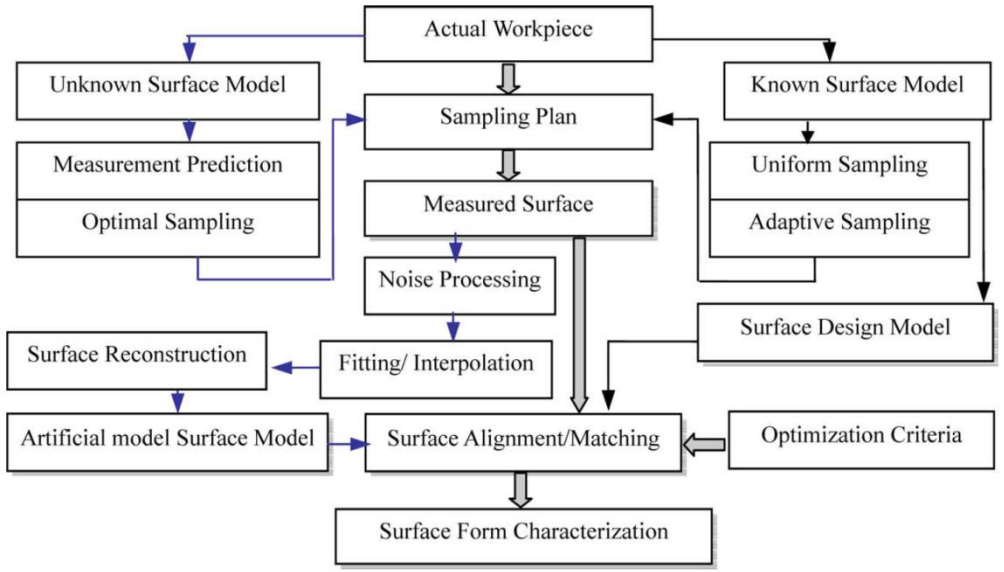

In this module, a series of evaluation algorithms and software for the evaluation of continuous freeform optical surfaces have been developed, such as the Integrated Freeform Characterization Method (IFCM) [26], the Robust Freeform measurement data involving outliers. The surface matching is conducted by the least squares method, and then the deviations between the design model and measured data are obtained. Then the outliers are located and processed by neighboring averaging or removal means, after which the surface matching

L. B. Kong, C. F. Cheung, W. B. Lee, and S. To. "An Integrated Manufacturing System for the Design, Fabrication, and Measurement of Ultra-Precision Freeform Optics." 244 IEEE TRANSACTIONS ON ELECTRONICS PACKAGING MANUFACTURING, VOL. 33, NO. 4, OCTOBER 2010.

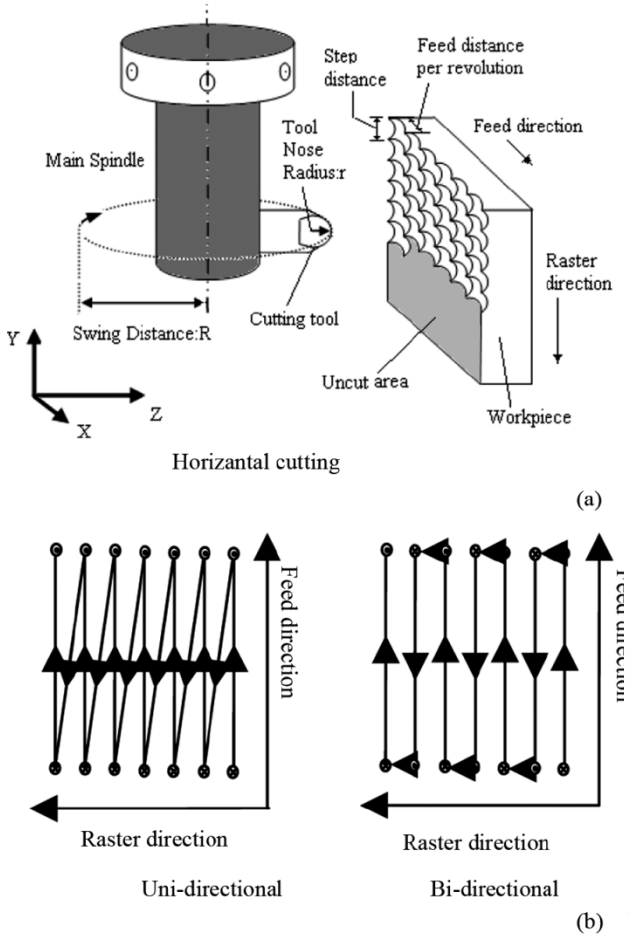

Fig. 4. Machining strategies for ultra-precision raster milling. (a) Cutting

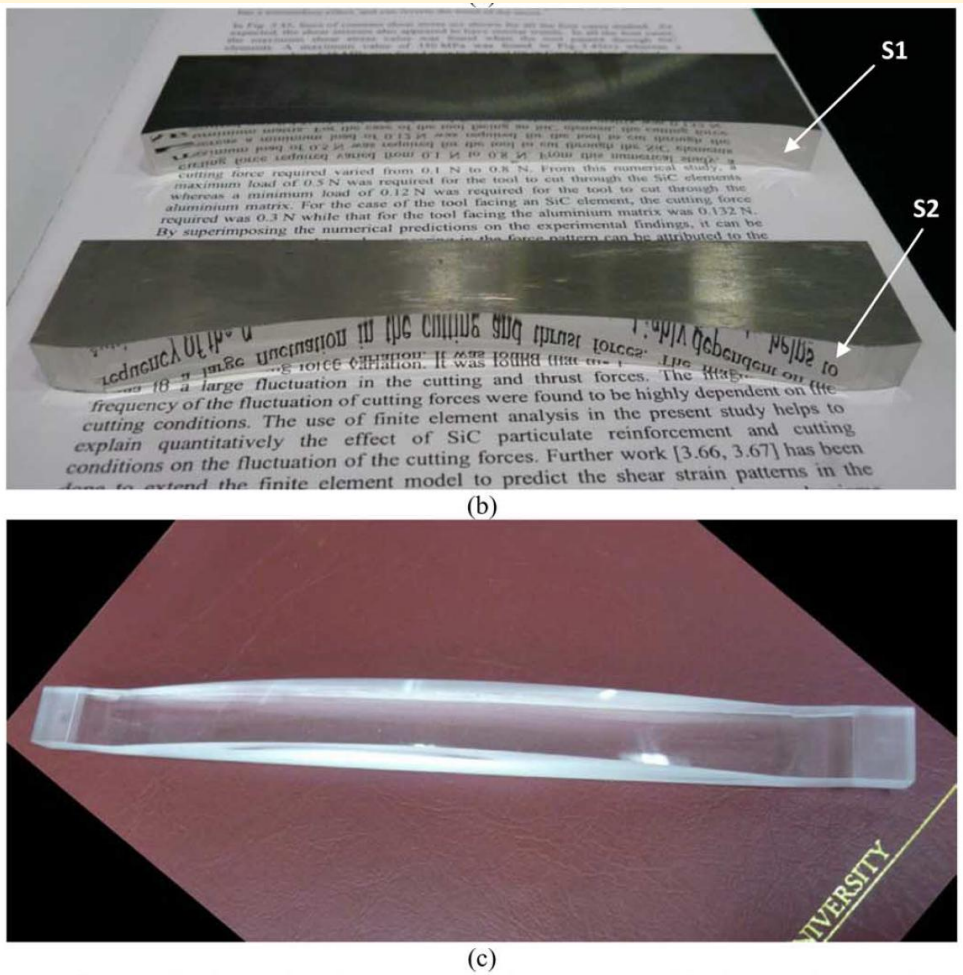

Fig. 11. Freeform application: F-theta lens. (a) F-theta lens CAD Specifications (unit: mm). (b) F-theta mould insert. (c) F-theta mould injection product.

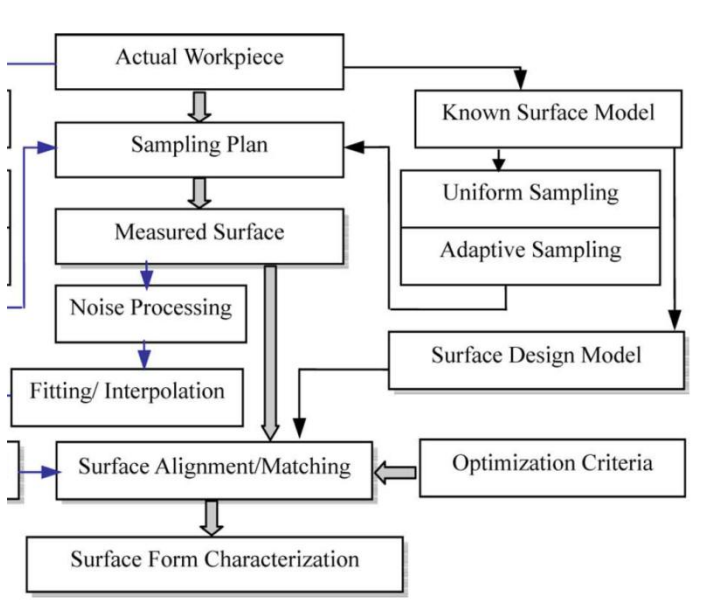

le, a series of evaluation algorithms and
evaluation of continuous freeform optical
n developed, such as the Integrated Freeform
Method (IFCM) [26], the Robust Freeform
ı involving outliers. The surface matching is
least squares method, and then the deviations
gn model and measured data are obtained.
are located and processed by neighboring
oval means, after which the surface matching

Ingo Sieber. " Design of freeform optics for an ophthalmological application." Proc. of SPIE Vol. 9131 913108-2.

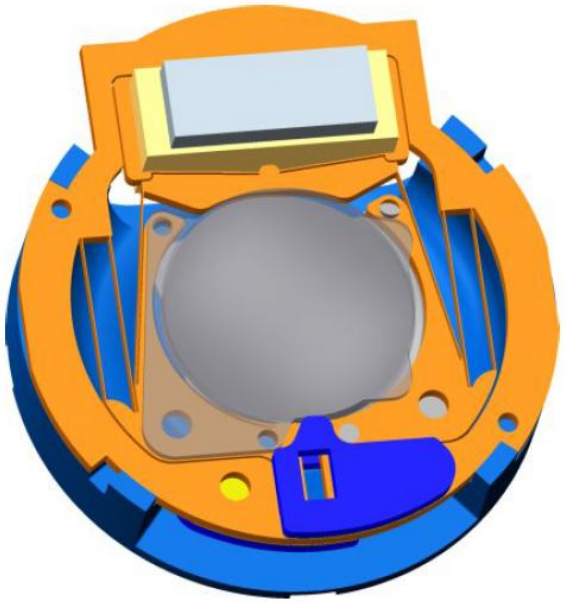

Figure 1. CAD model of the active optical element (combination of adjustable optics, piezo actuator, and silicon linkage) [16].

Ingo Sieber. " Design of freeform optics for an ophthalmological application." Proc. of SPIE Vol. 9131 913108-2.

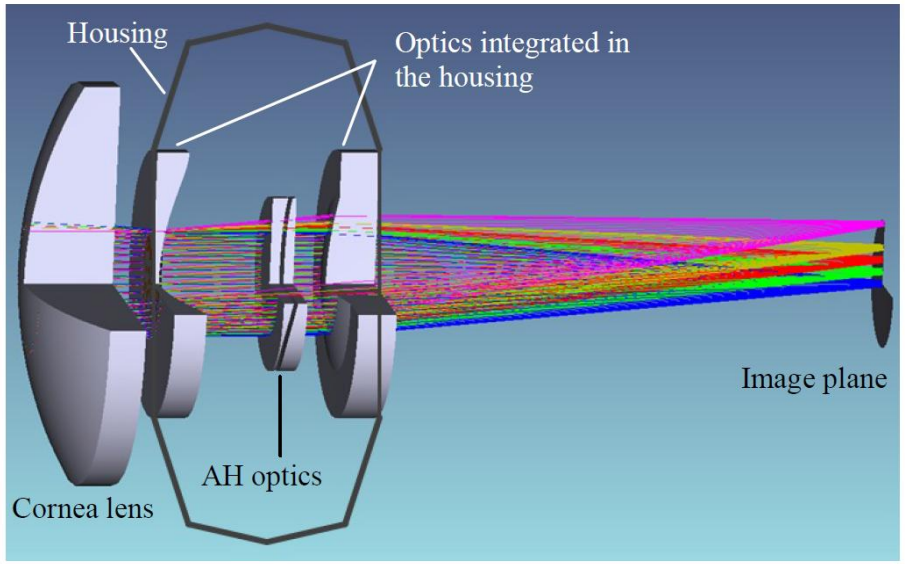

Figure 3. Optical subsystem of the demonstrator of the Artificial Accommodation System. The cornea lens, a sketch of the housing with the integrated optics, the AH optics, and the image plane are shown.

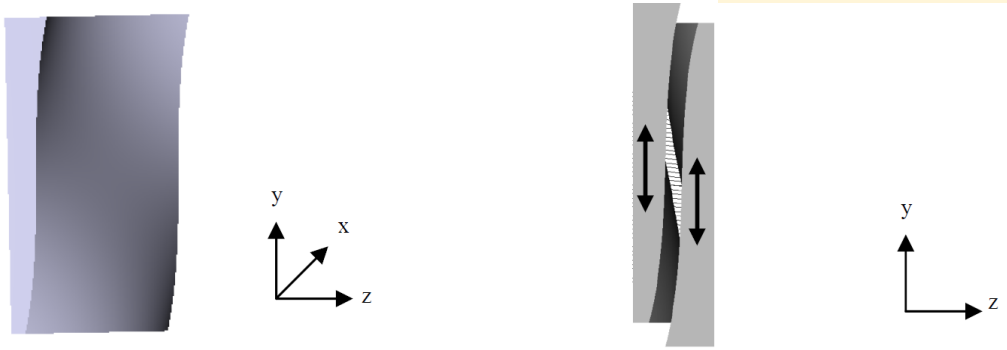

Figure 4. Example of an Alvarez-Humphrey surface (left). On the right, the variation of the refraction power by means of a shift of the Alvarez-Humphrey surfaces perpendicular to the optical axes (z-axes in the figure) is shown.

Figure 1. CAD model of the active optical element (combination of adjustable optics, piezo actuator, and silicon linkage) [16].

Likai Li. " Fabrication of microinjection-molded miniature freeform Alvarez lenses." Received 24 March 2014; revised 26 May 2014; accepted 27 May 2014; posted 29 May 2014 (Doc. ID 208449); published 30 June 2014.

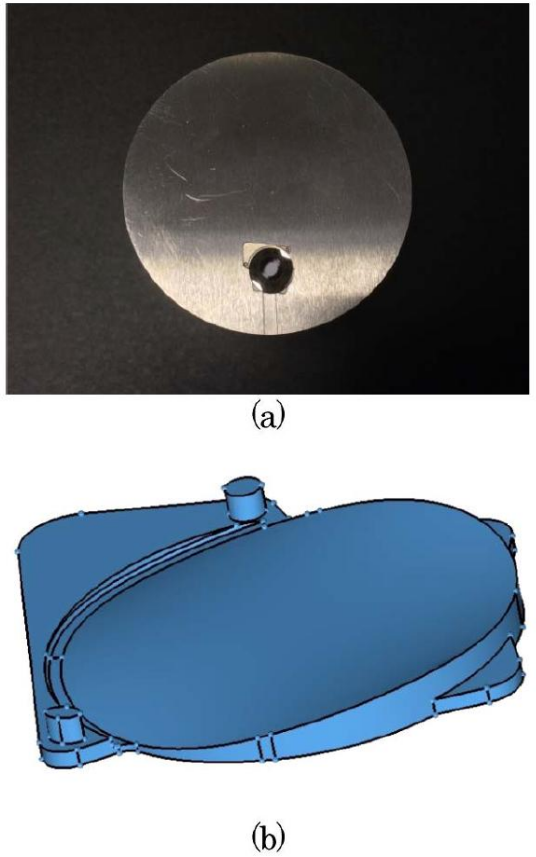

Fig. 2. (a) Finished ultraprecision diamond-machined mold for injection molding. (b) 3D model of the molded Alvarez lens with small straight pins and flats designed for assembly.

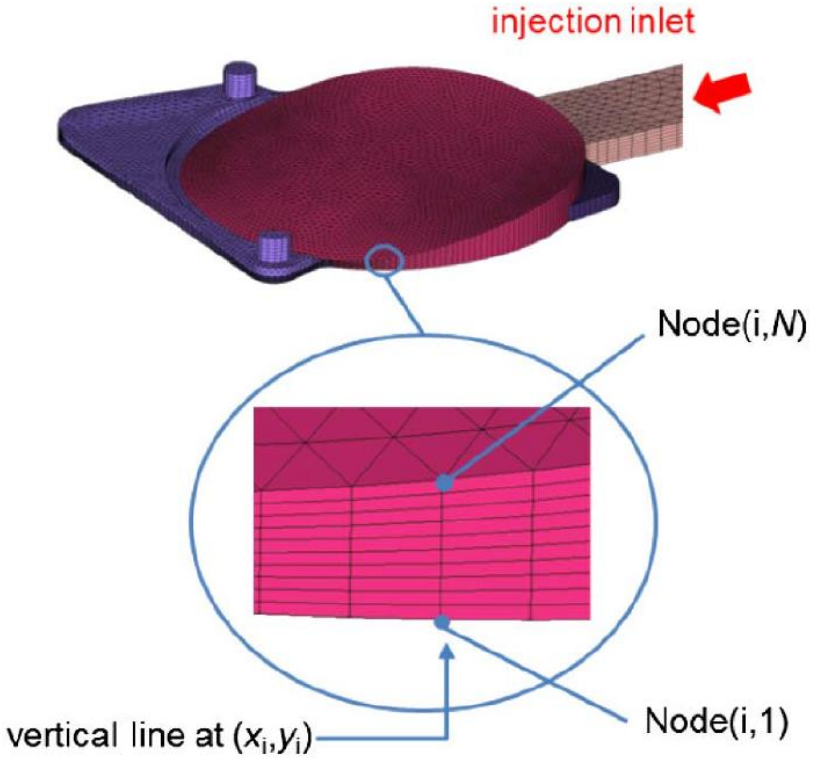

Fig. 4. FEM mesh model of the Alvarez lens. Node $(i, 1)$ is numbered along the vertical line at coordinates (x_i, y_i) at the bottom surface, and Node (i, N) is the node along the vertical line at coordinates (x_i, y_i) at its top surface.

asphericon (www.asphericon.com)

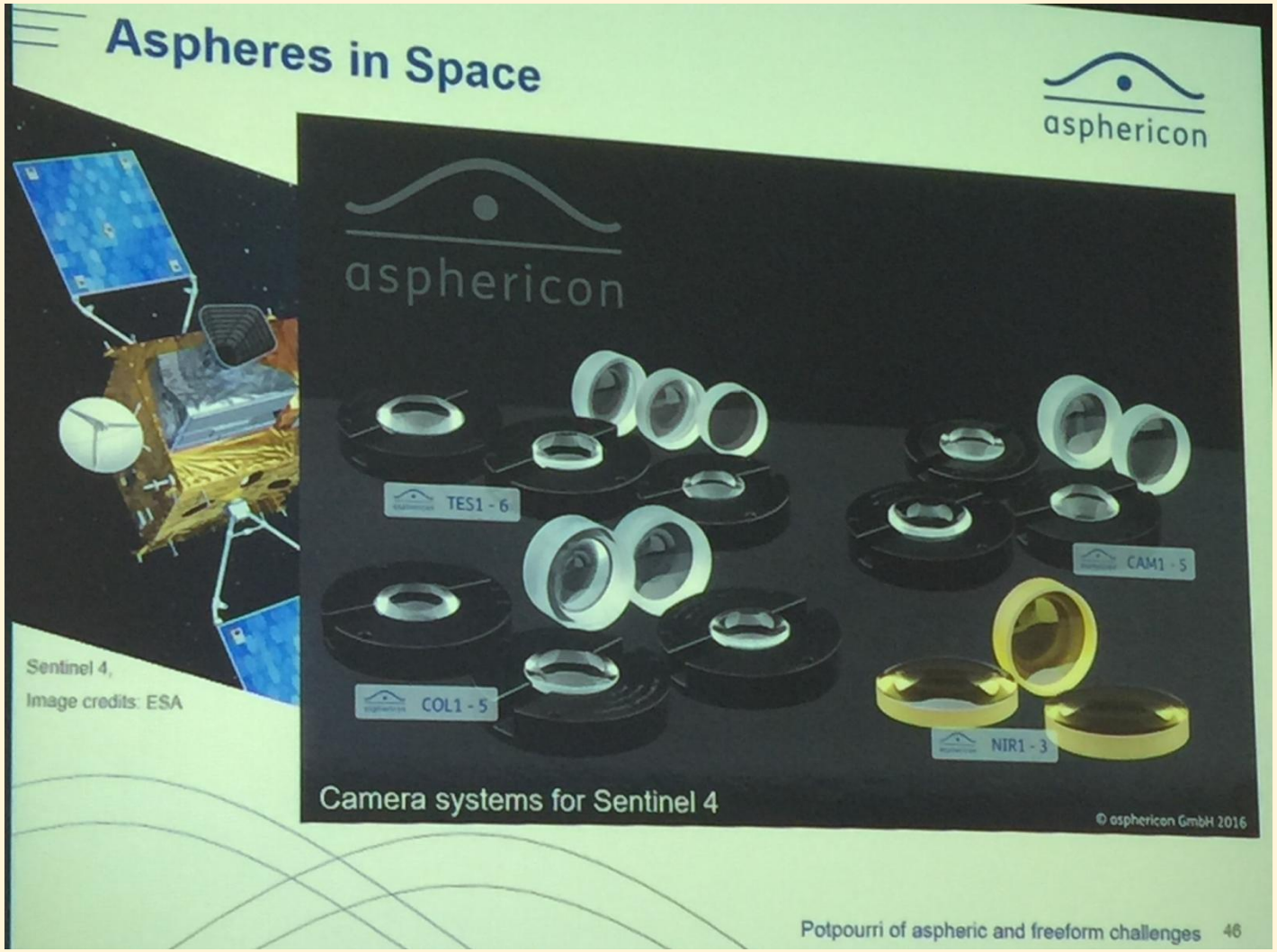

asphericon (www.asphericon.com)

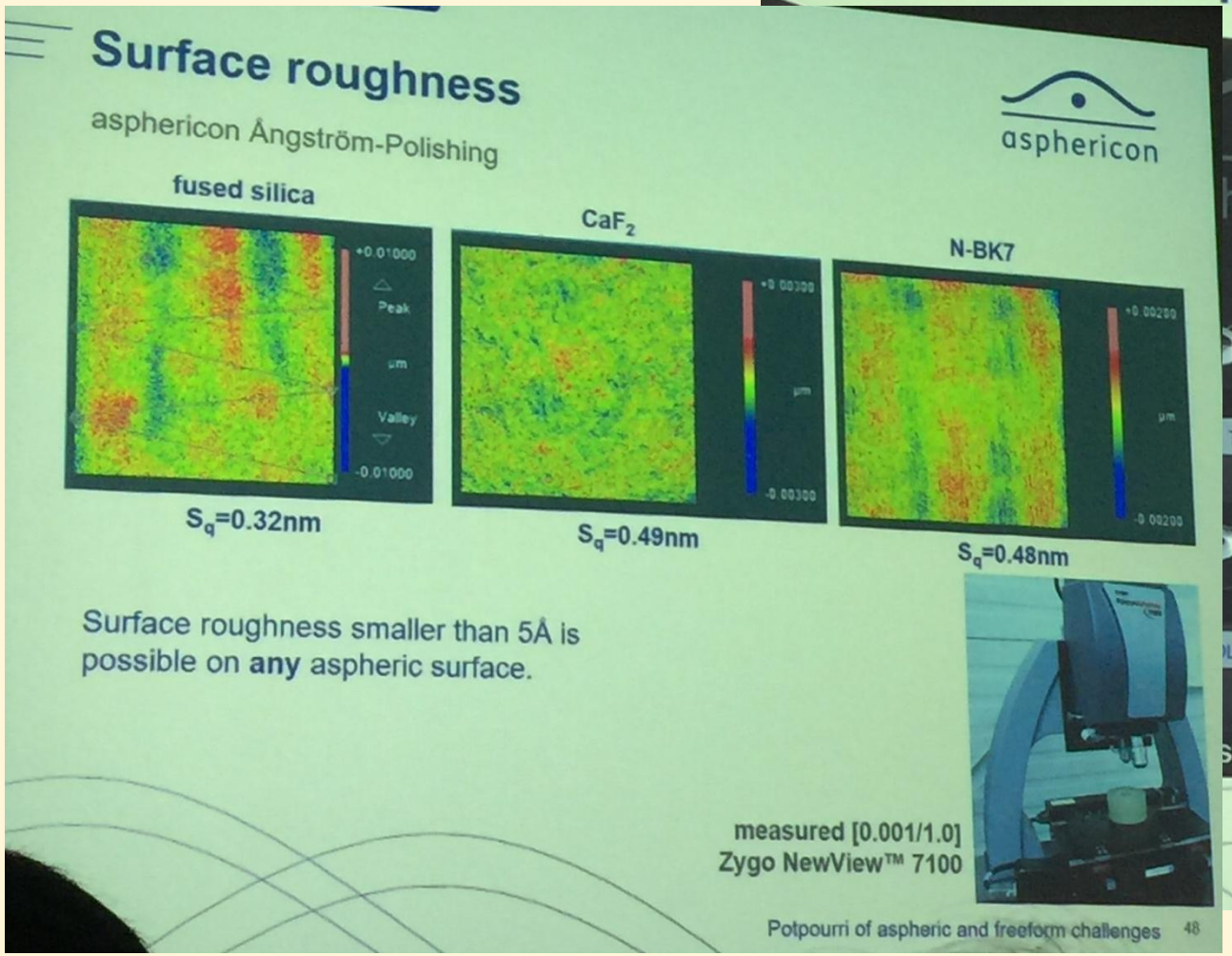

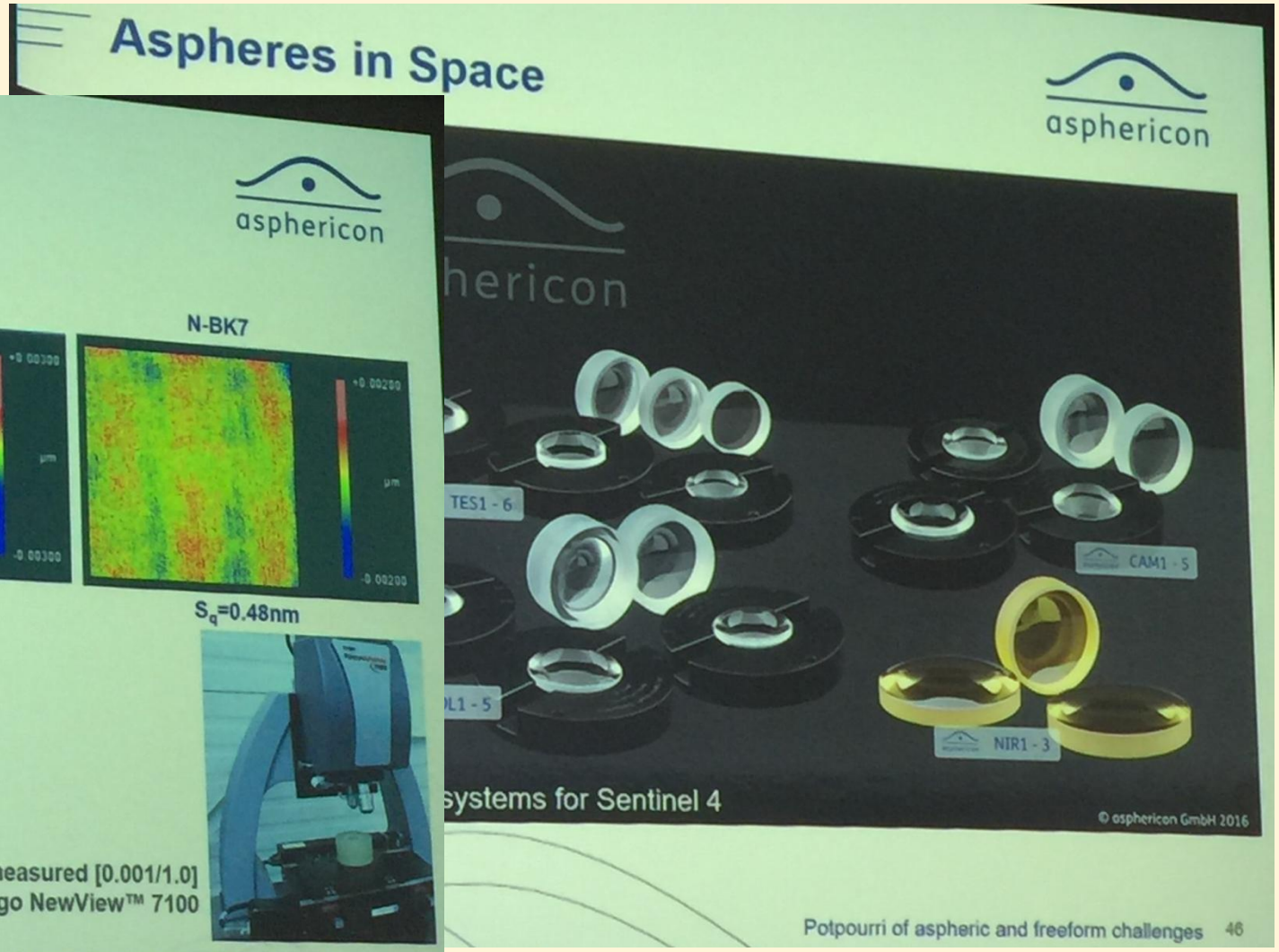

asphericon (www.asphericon.com)

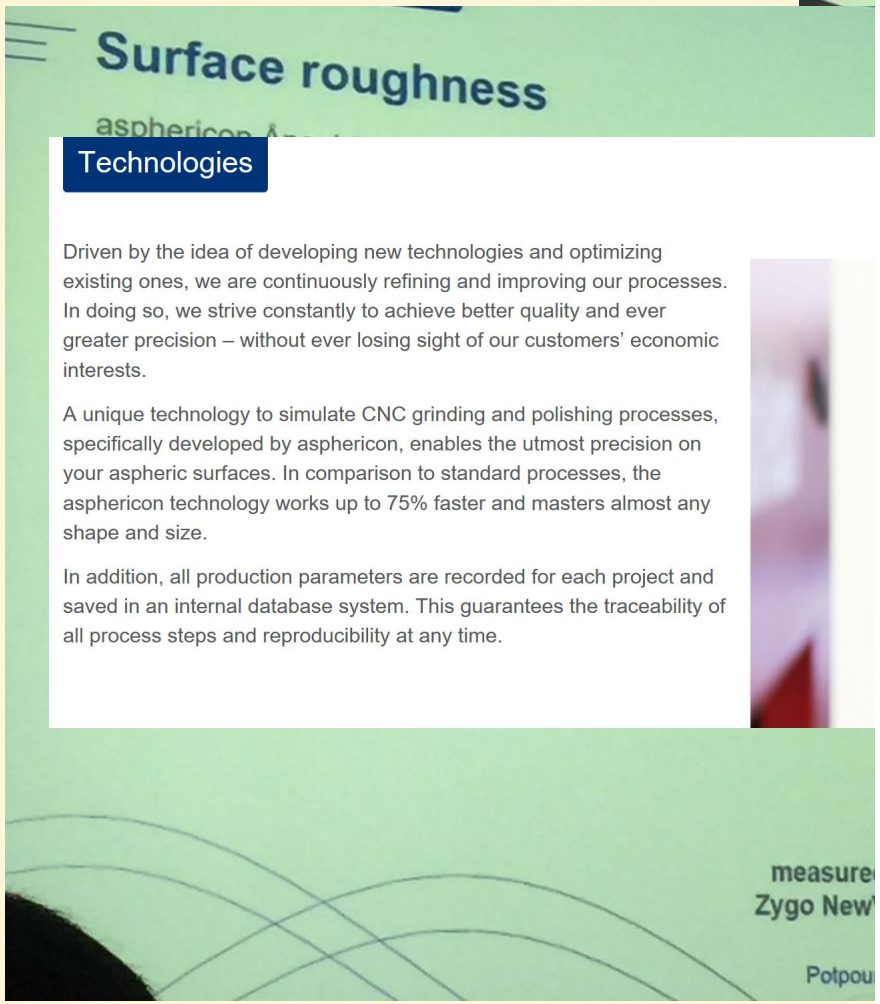

Diamond turning

Ultra-precise cutting using monocrystalline diamond is the key technology for manufacturing virtually any optical functional surface with the utmost precision. This enables the processing of non-ferrous metals, nickel-phosphorus coatings, plastics, crystals and IR lenses.

Manufacturing dimensions [ISO 10110-1]		
Achievable diameters	mm	1 - 420
Center thickness	mm	from 0.5[1]
Surface shape [ISO 10110-1; 12]		**up to**
Irregularity – B (PV)[2]	nm	100
RMS irregularity – RMSi – D	nm	20
Surface roughness – Rq	nm	1

1 Depends on diameter and material
2 Often also called the PV - error of the measured surface. Means the total surface deviation corrected for Sagitta error (power).

Available technologies

- Diamond turning with 2 and 3 linear axes
- Fly cutting
- Slow tool servo

Processable materials

- Copper, aluminum, brass, nickel silver, nickel
- Nickel-phosphorus layers
- Polycarbonate, PMMA
- Silicon, germanium, zinc sulfide
- IR lenses

Achievable optical component geometries

- Aspheres
- Spheres
- Cylinders
- Toroids
- Microlenses
- Fresnel structures
- Diffractive optical elements
- Freeforms

asphericon (www.asphericon.com)

Technologies

Driven by the idea of developing new technologies and optimizing existing ones, we are continuously refining and improving our processes. In doing so, we strive constantly to achieve better quality and ever greater precision – without ever losing sight of our customers' economic interests.

A unique technology to simulate CNC grinding and polishing processes, specifically developed by asphericon, enables the utmost precision on your aspheric surfaces. In comparison to standard processes, the asphericon technology works up to 75% faster and masters almost any shape and size.

In addition, all production parameters are recorded for each project and saved in an internal database system. This guarantees the traceability of all process steps and reproducibility at any time.

Diamond turning

Ultra-precise cutting using monocrystalline diamond is the key technology for manufacturing virtually any optical functional surface with the utmost precision. This enables the processing of non-ferrous metals, nickel-phosphorus coatings, plastics, crystals and IR lenses.

- Aspheres
- Spheres
- Cylinders
- Toroids
- Microlenses
- Fresnel structures
- Diffractive optical elements
- Freeforms

Lee, W. M., Avinash Upadhya, and Tri Phan. "Mobile microscopy on the move." *IS&T/SPIE Electronic Imaging*. International Society for Optics and Photonics, 2014.

Lee, W. M., et al. "Fabricating low cost and high performance elastomer lenses using hanging droplets." *Biomedical optics express* 5.5 (2014): 1626-1635.

- Hanging droplet method
- Focal lengths from 1 mm to 15 mm

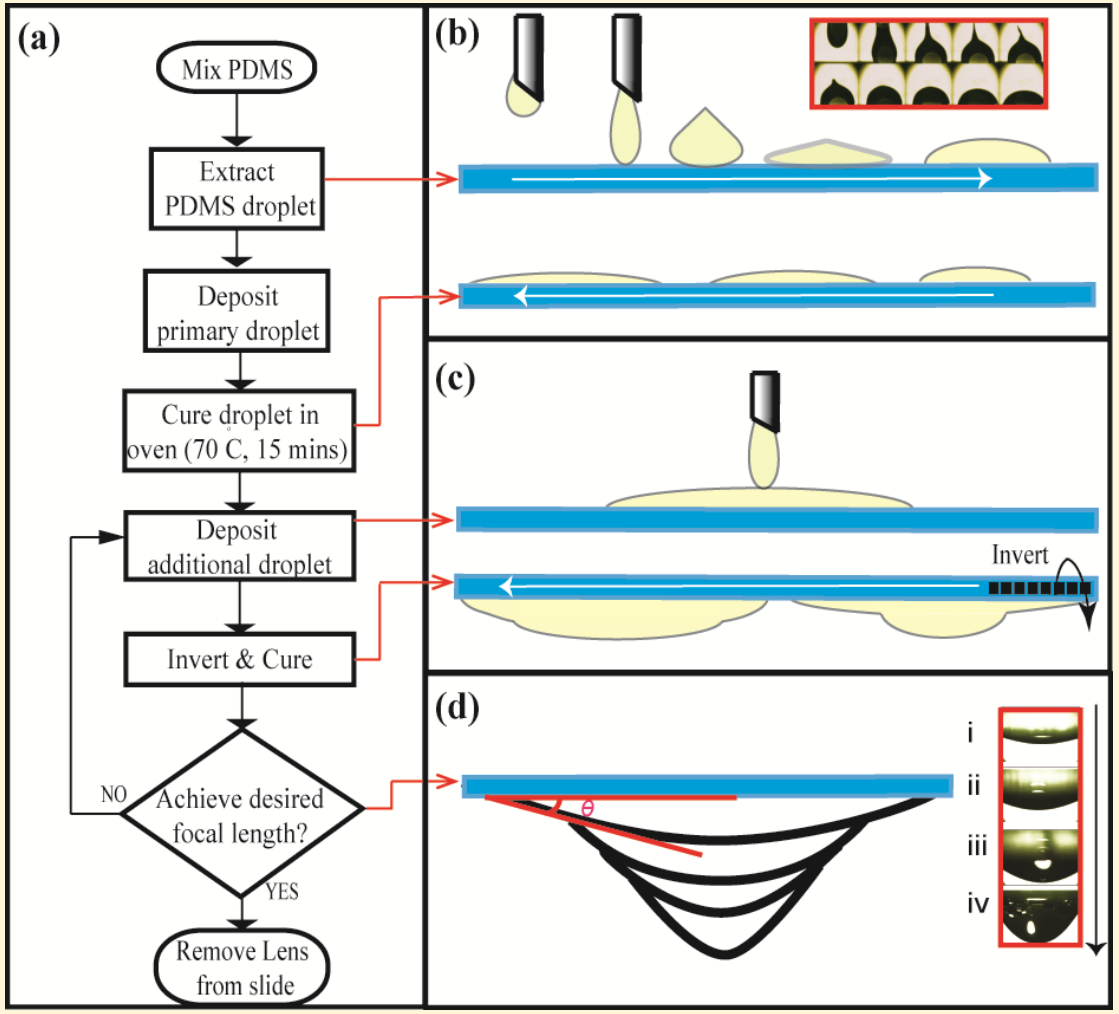

Lee, W. M., Avinash Upadhya, and Tri Phan. "Mobile microscopy on the move." *IS&T/SPIE Electronic Imaging*. International Society for Optics and Photonics, 2014.

Lee, W. M., et al. "Fabricating low cost and high performance elastomer lenses using hanging droplets." *Biomedical optics express* 5.5 (2014): 1626-1635.

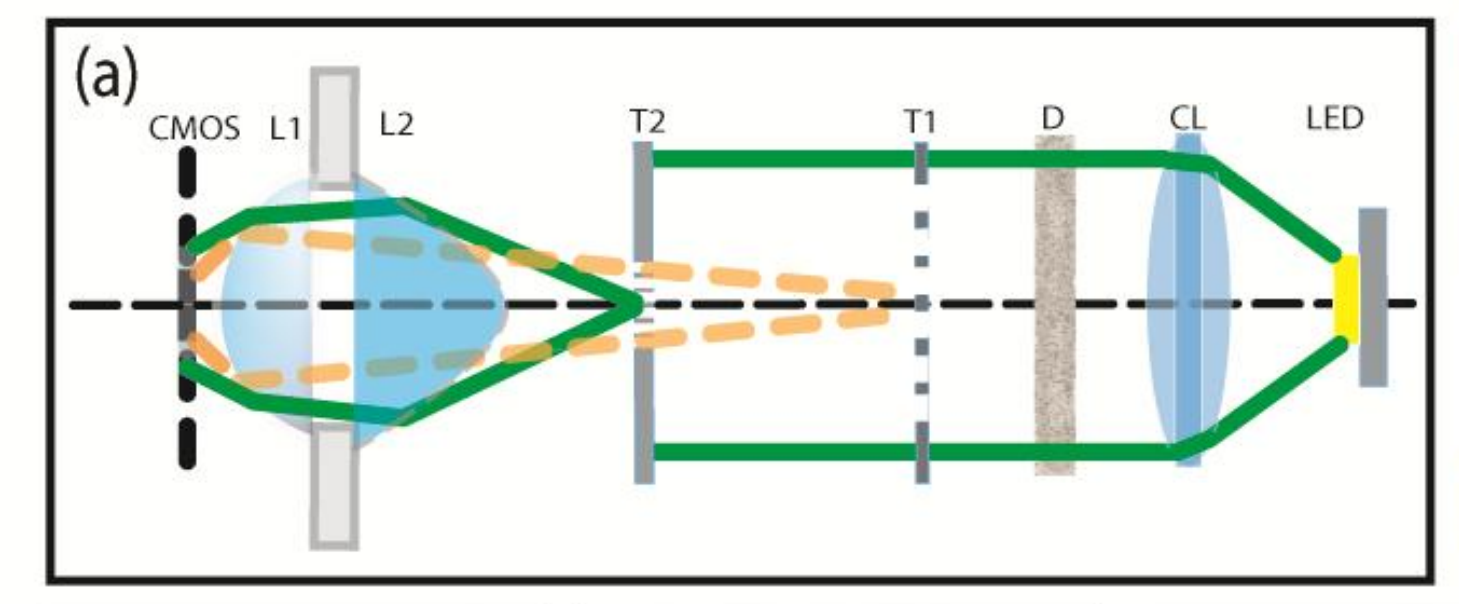

Lee, W. M., Avinash Upadhya, and Tri Phan. "Mobile microscopy on the move." *IS&T/SPIE Electronic Imaging*. International Society for Optics and Photonics, 2014.

Lee, W. M., et al. "Fabricating low cost and high performance elastomer lenses using hanging droplets." *Biomedical optics express* 5.5 (2014): 1626-1635.

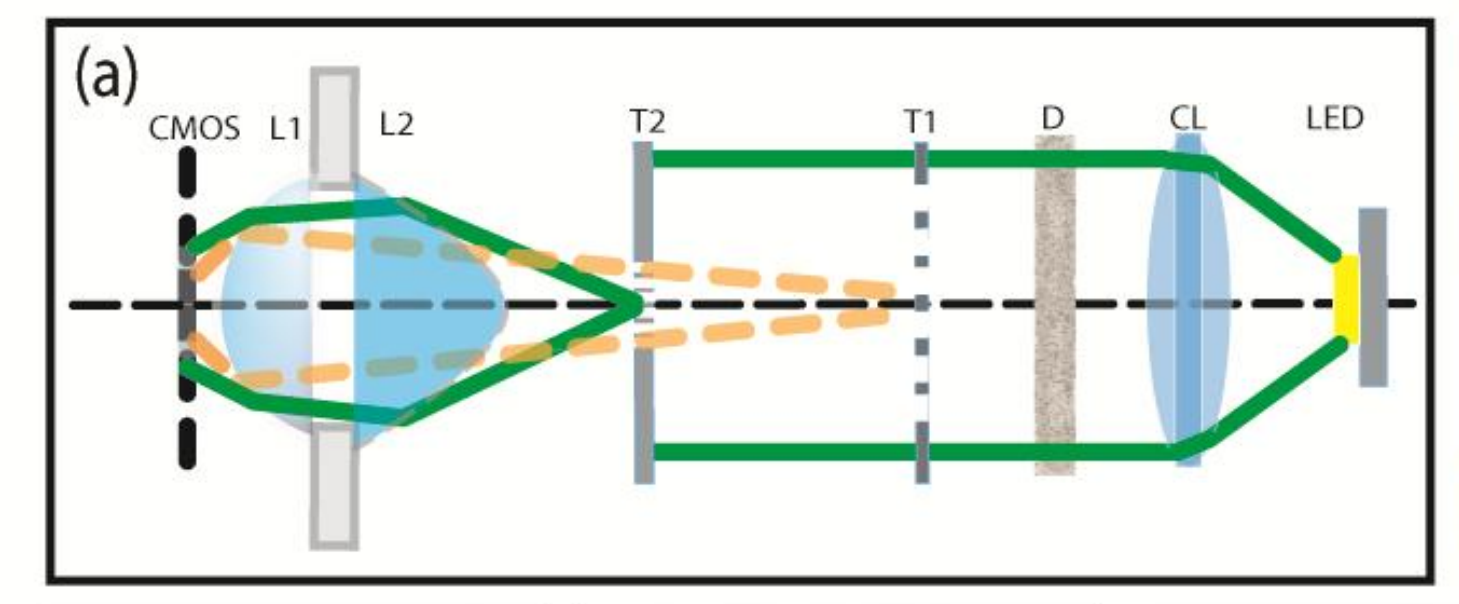

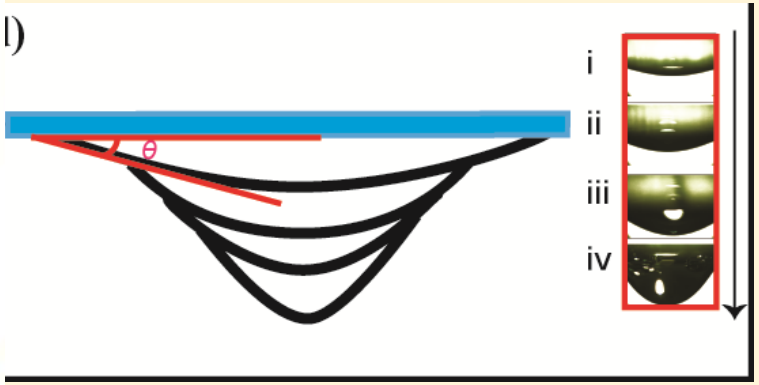

Lee, W. M., Avinash Upadhya, and Tri Phan. "Mobile microscopy on the move." *IS&T/SPIE Electronic Imaging*. International Society for Optics and Photonics, 2014.

Lee, W. M., et al. "Fabricating low cost and high performance elastomer lenses using hanging droplets." *Biomedical optics express* 5.5 (2014): 1626-1635.

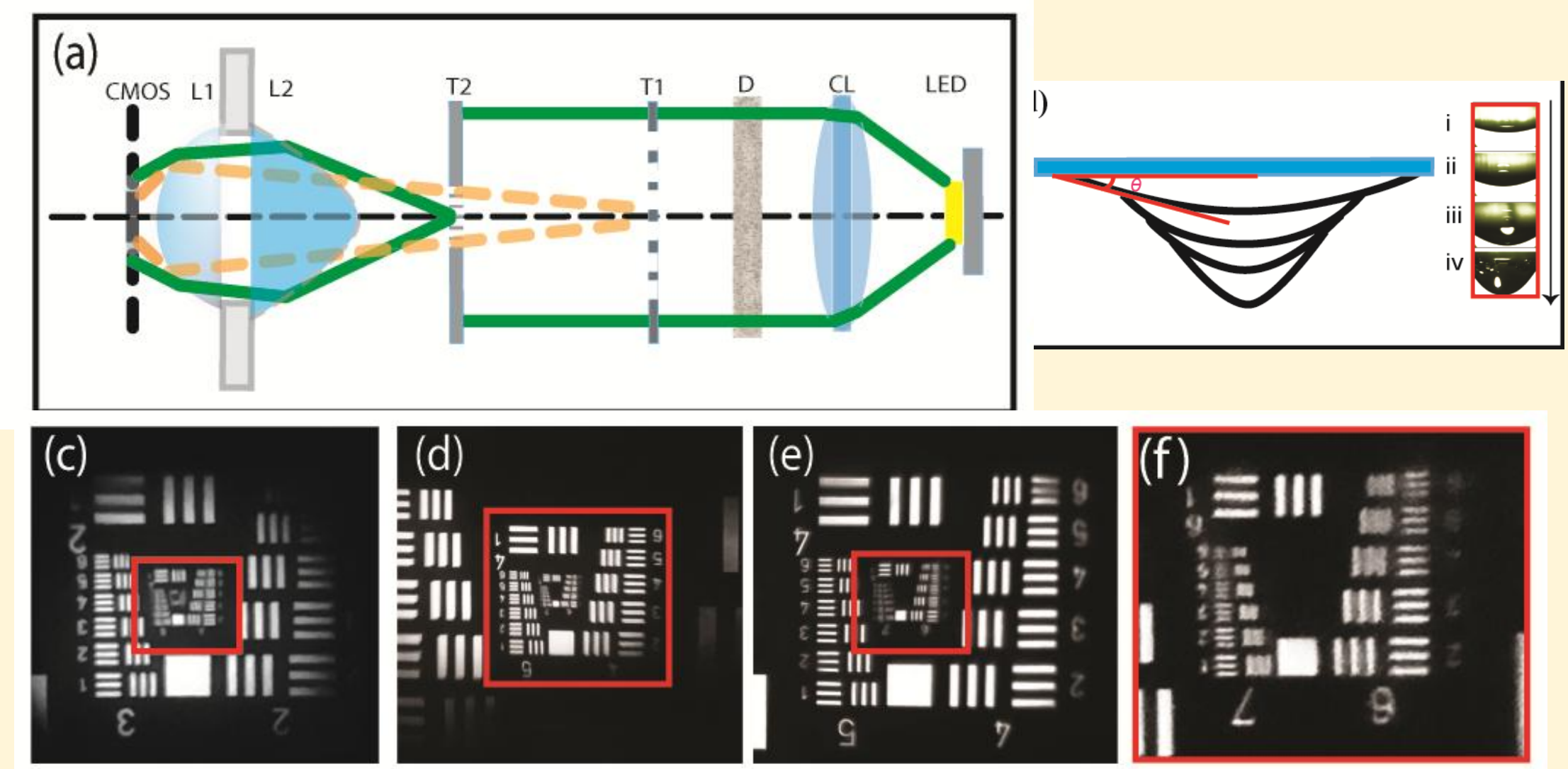

Jens Dunkel. " Fabrication of microoptical freeform arrays on wafer level for imaging applications."*Fraunhofer Institute for Applied Optics and Precision Engineering, A.-Einstein-Str. 7, 07745 Jena, Germany.*

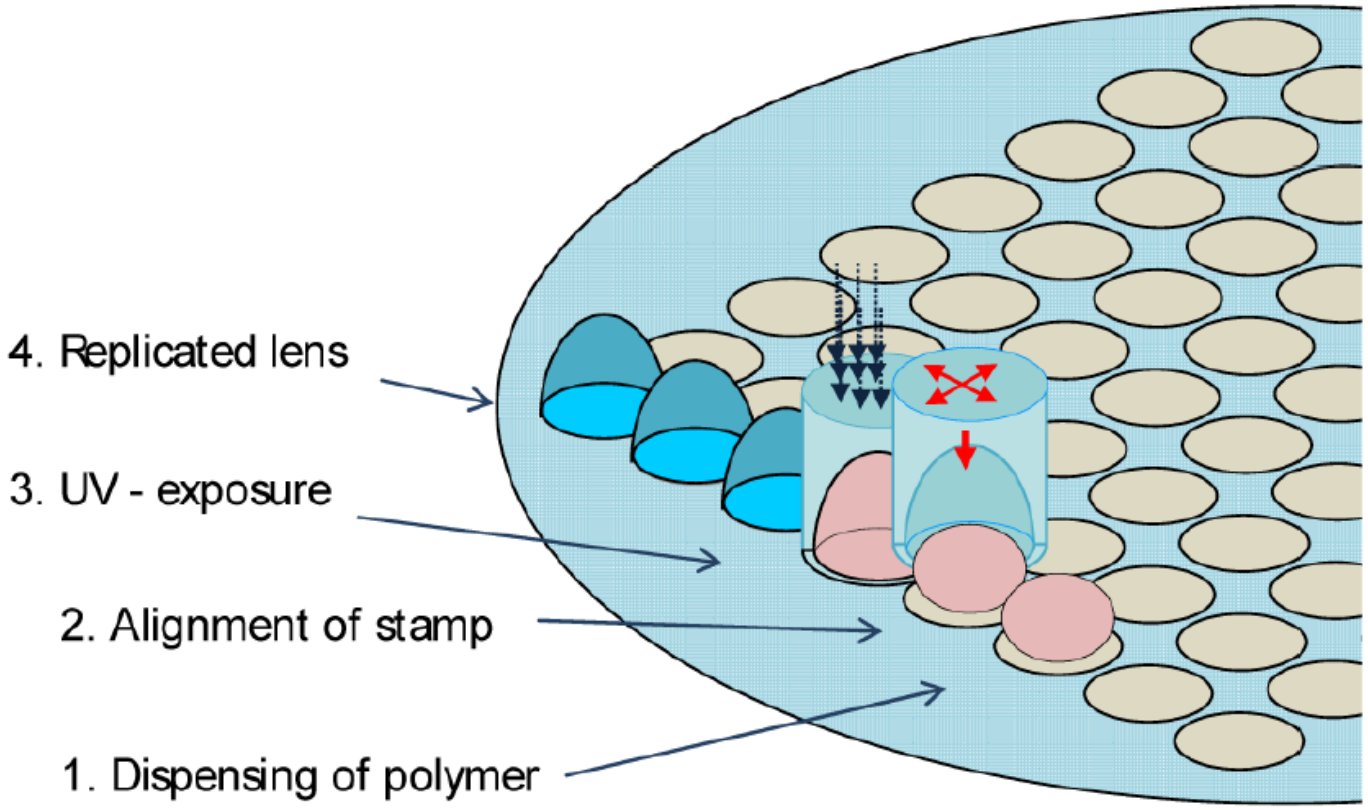

Fig. 4. Schematic representation of the step and repeat micro imprint process.

Jens Dunkel. " Fabrication of microoptical freeform arrays on wafer level for imaging applications."*Fraunhofer Institute for Applied Optics and Precision Engineering, A.-Einstein-Str. 7, 07745 Jena, Germany*

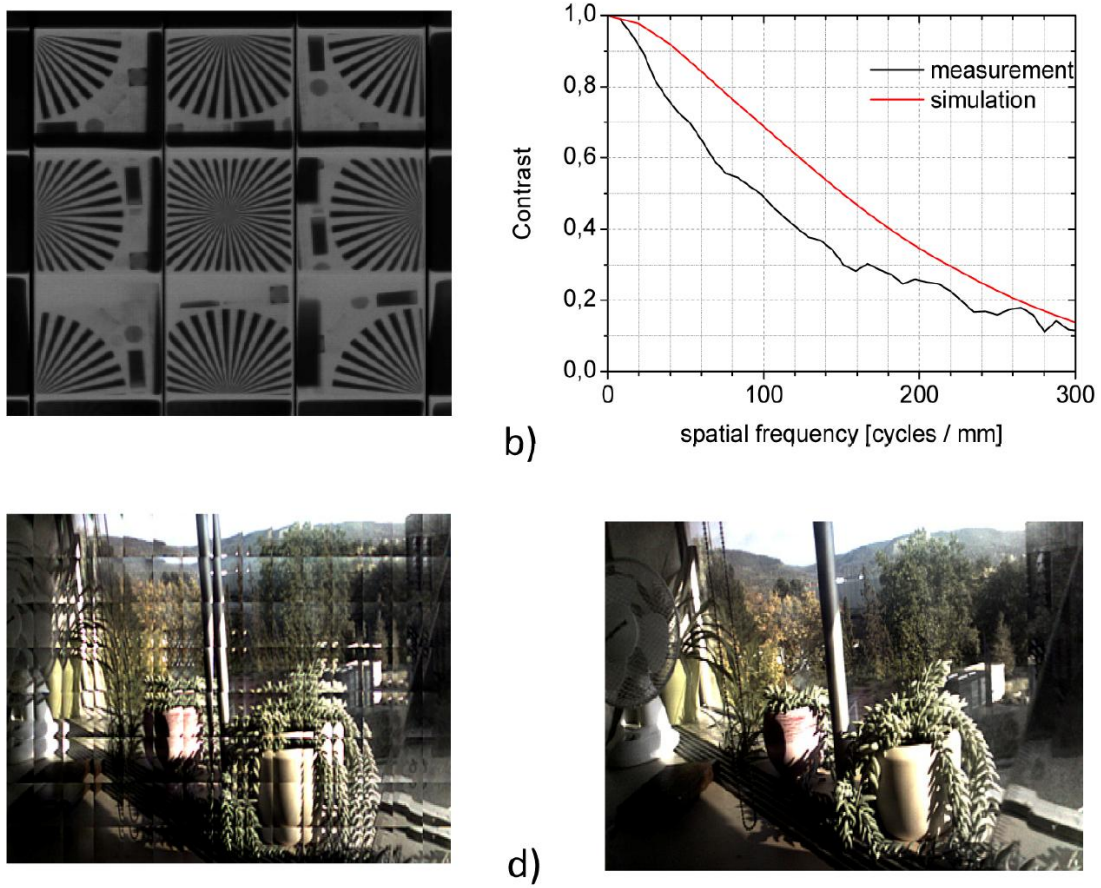

Fig. 11. Image of Siemens star test target captured by 3 x 3 channels (a), measurement of the modulation transfer function of the central channel in comparison to simulation data (b), raw image consisting of 15 x 9 subimages (c) and reconstructed final image of camera demonstrator (d).

(www.luxexcel.com)

- In collaboration with Luxexcel, our group will further develop the Printoptical® technology towards smaller features and more accurate surface control, larger selection of materials, novel optics and unique combination with other state-of-the-art micro-optics and nano photonics manufacturing methods as well as mechanics, electronics and biocompatible materials.

te
otonics

lop the Printoptical®
urface control, larger selection of
r state-of-the-art micro-optics
echanics, electronics and

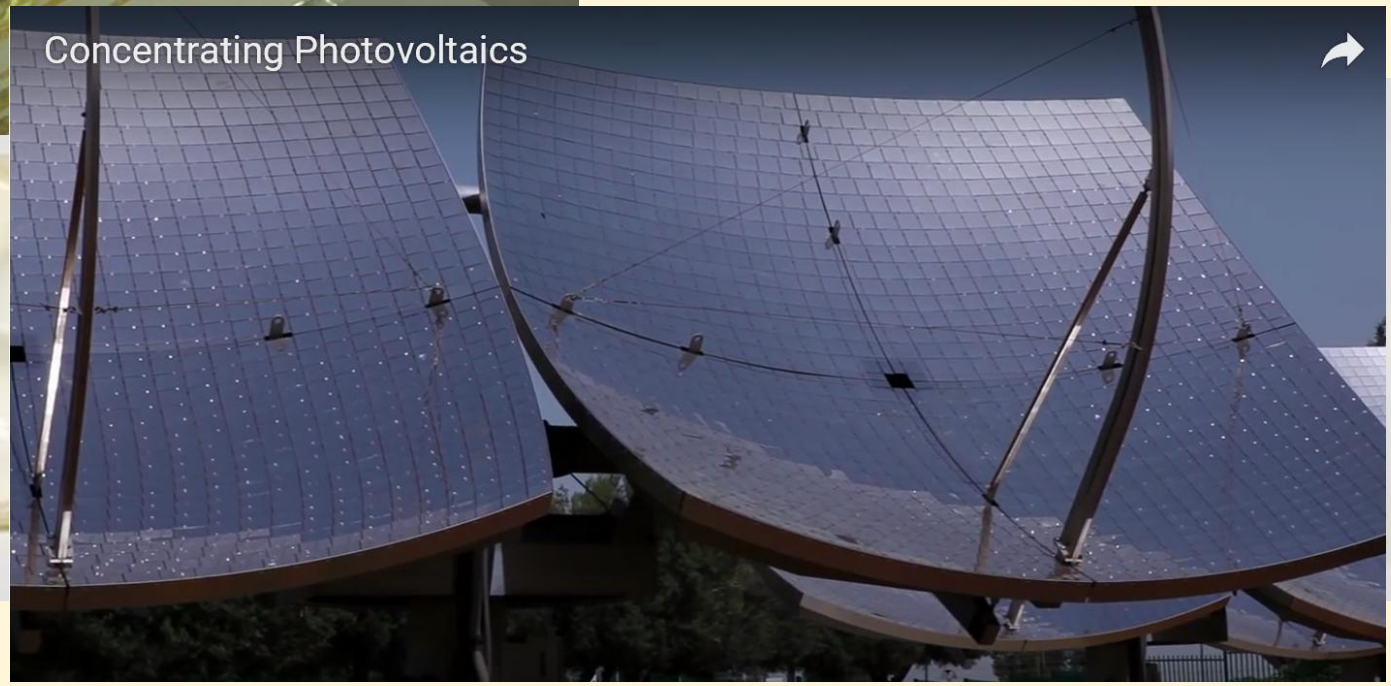

te
otonics

optical®
l, larger selection of
e-art micro-optics
ctronics and

EASY LED
IDMAN
LUXEXCEL®
Millog
nanobakers
THIN FOIL OPTICS
NANOCOMP
oplatek
ThermoFisher SCIENTIFIC
VAISALA
XAAR®

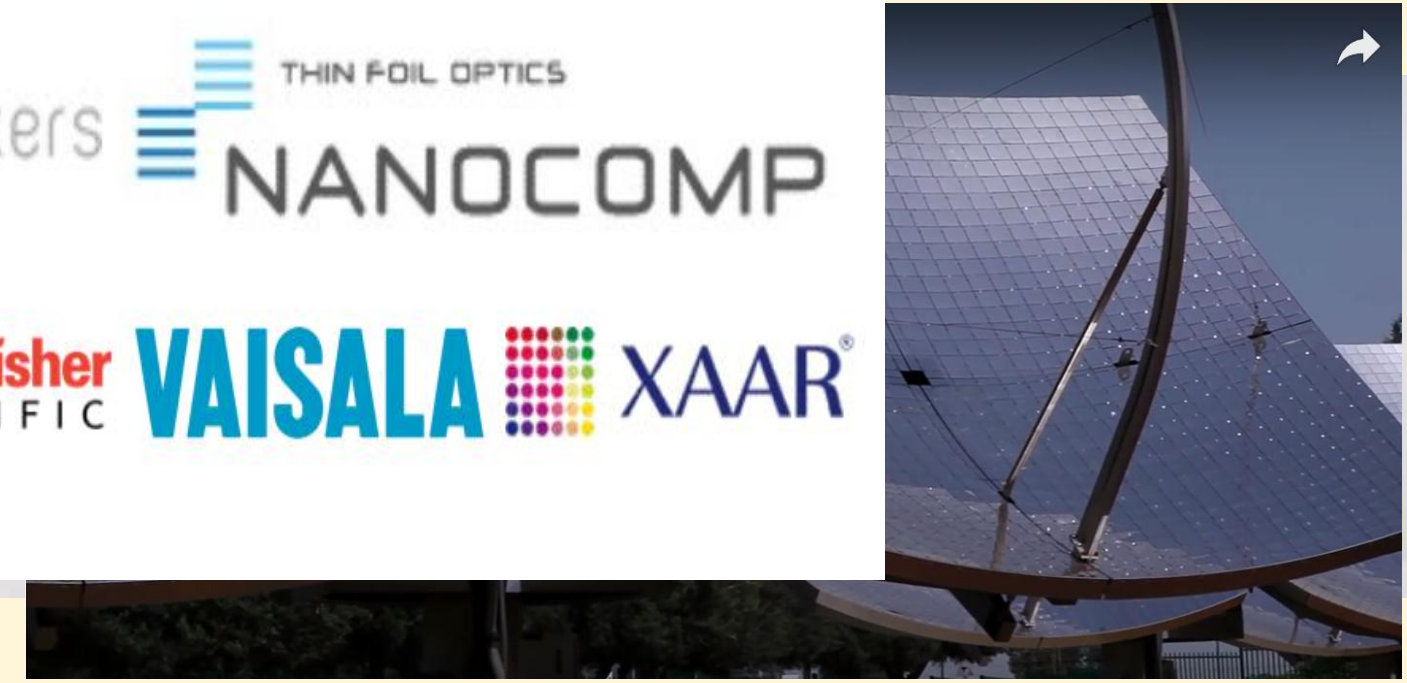

(www.nanoscribe.com)

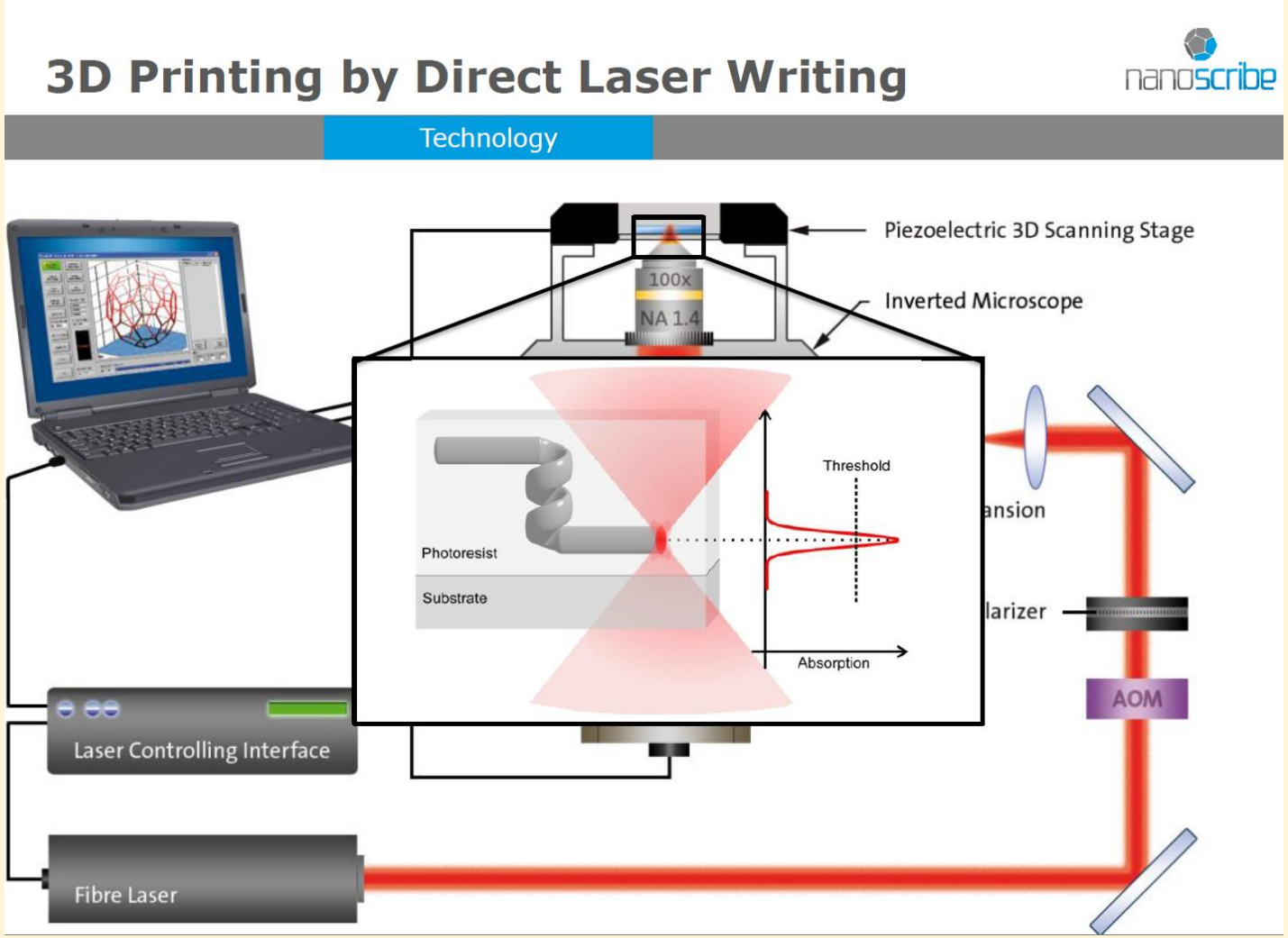

nanoscribe

(www.nanoscribe.com)

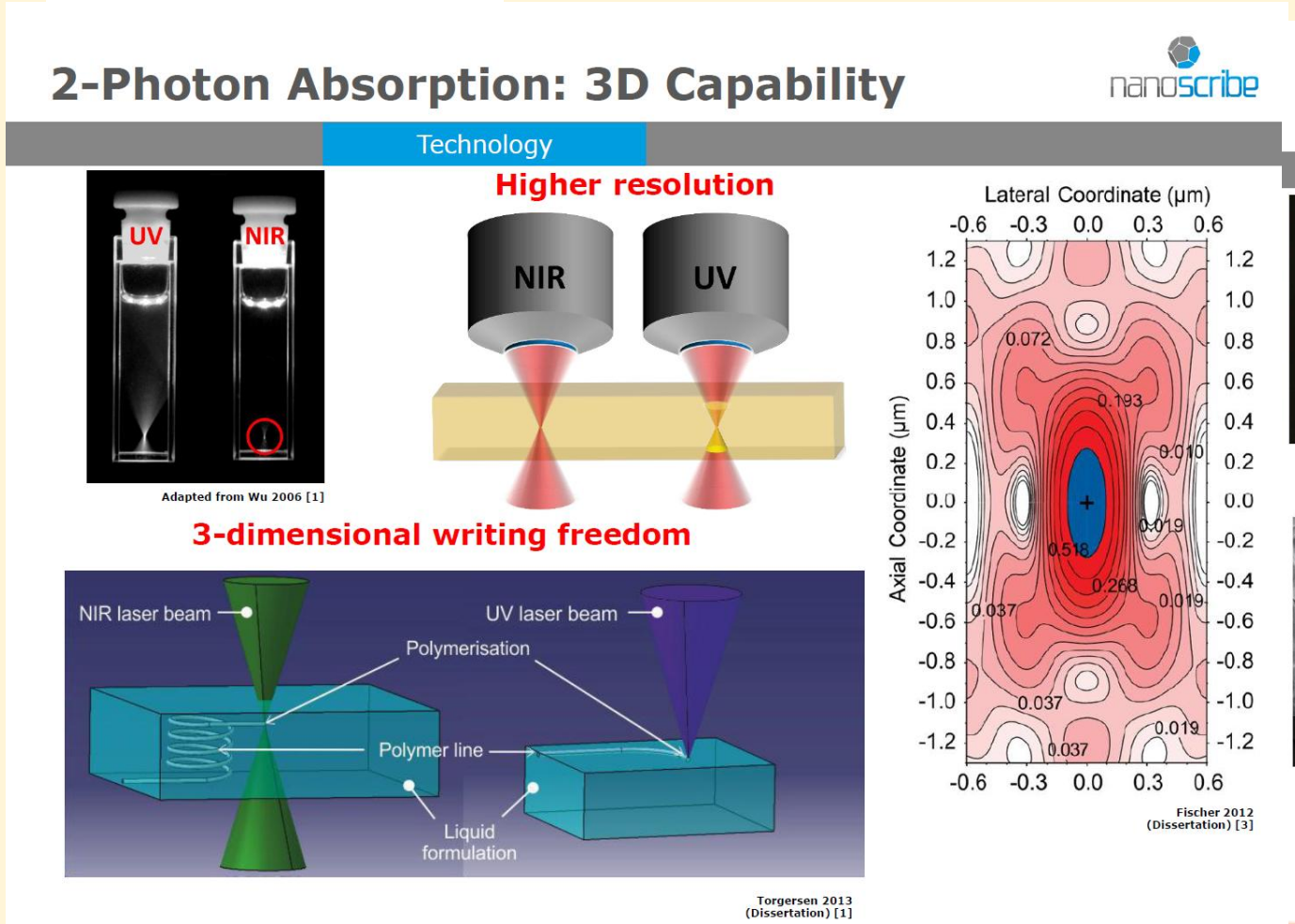

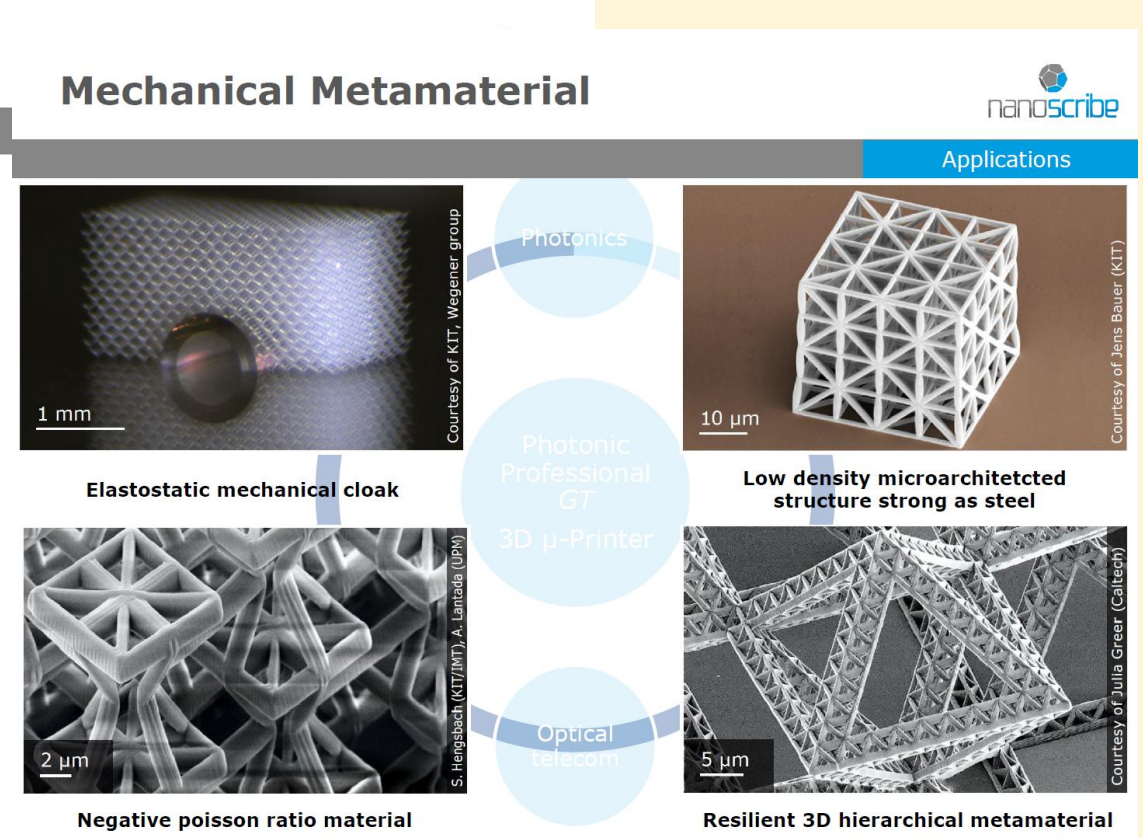

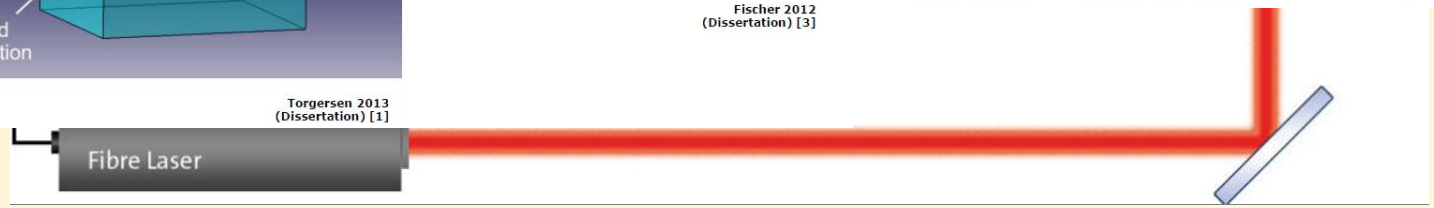

Zehua Qu. "*The design of double electrostatic-lens optics for resonance enhanced multiphoton ionization and photoelectron imaging experiments.*"Received 9 December 2014; accepted 2 June 2015; published online 16 June 2015).

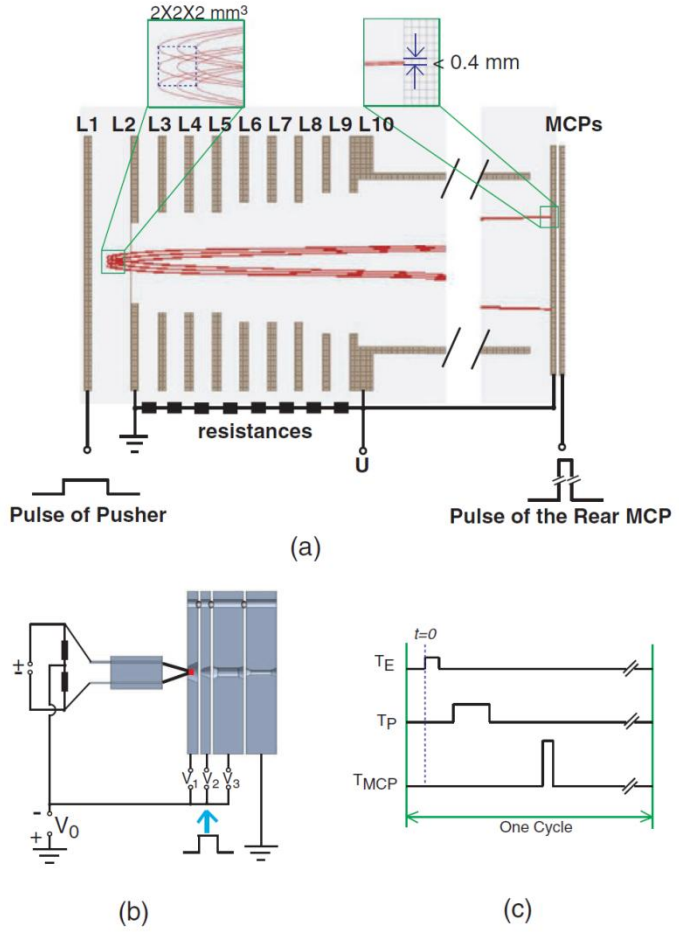

FIG. 2. (Color online) (a) The simulation of ion optics assembly and the detector setup. (b) Pulsed electron gun arrangement. (c) Timing sequence used in the experiments.

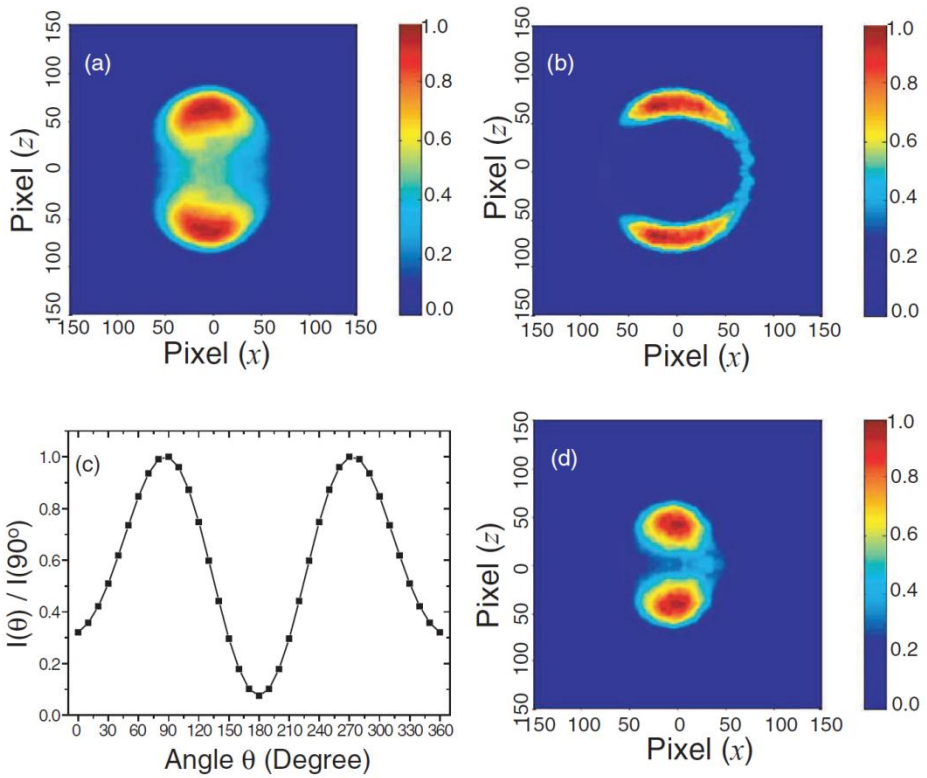

FIG. 5. (Color online) Dissociative electron attachment to NO. (a) 2D image at the electron incident energy of 8.3 eV. (b) The sliced image of O^- ions at the electron incident energy of 8.3eV. (c) The angular distribution plot of O^- with the kinetic energies of 0.4–0.7 eV [obtained from the sliced image (b)]. (d) The sliced image of O^- ions at the electron incident energy of 7.3 eV. The electron incident direction is from left to right. In the images, the ion intensities are normalized with their respective highest values.

Zehua Qu. "*The design of double electrostatic-lens optics for resonance enhanced multiphoton ionization and photoelectron imaging experiments.*"Received 9 December 2014; accepted 2 June 2015; published online 16 June 2015).

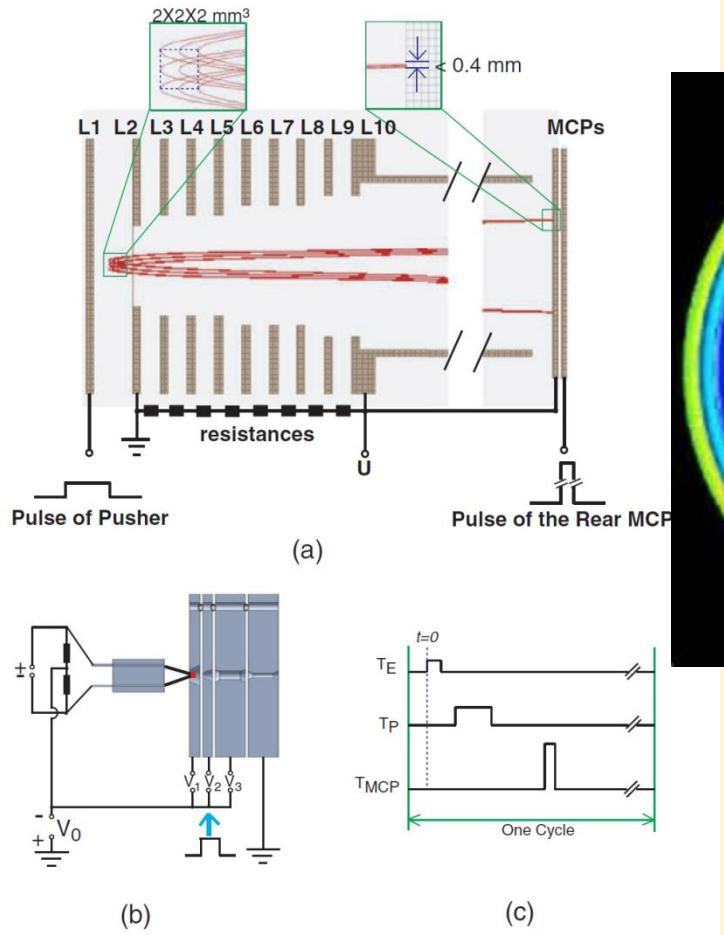

FIG. 2. (Color online) (a) The simulation of ion optics assembly and the detector setup. (b) Pulsed electron gun arrangement. (c) Timing sequence used in the experiments.

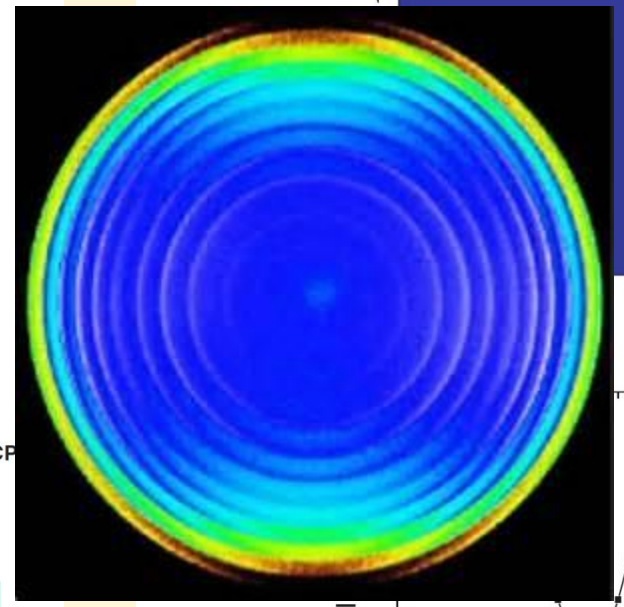

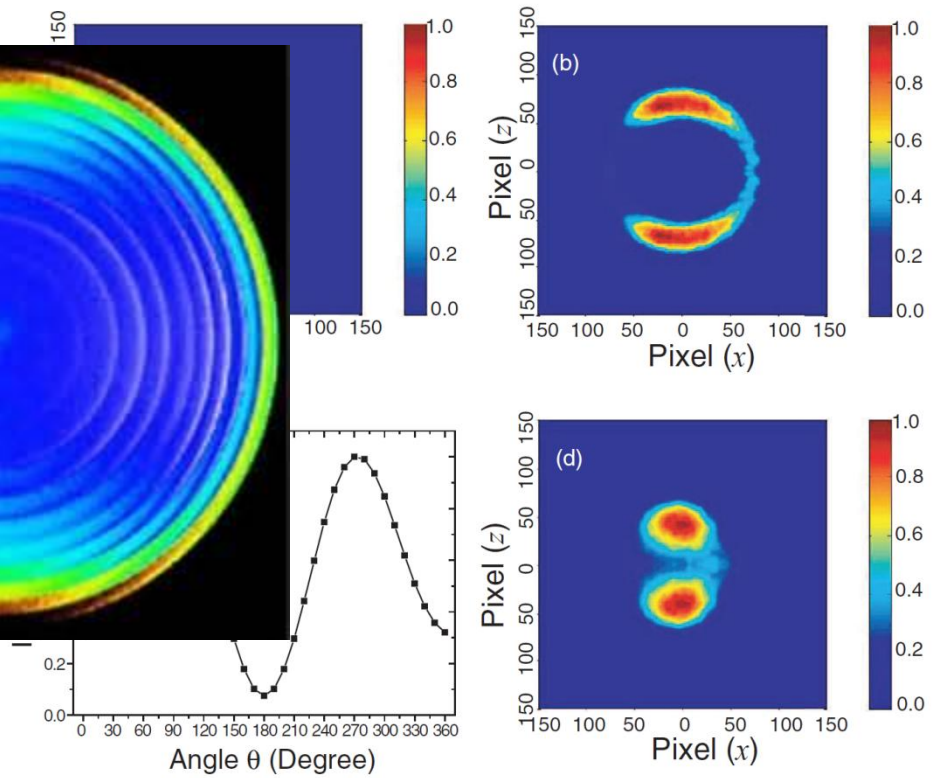

FIG. 5. (Color online) Dissociative electron attachment to NO. (a) 2D image at the electron incident energy of 8.3 eV. (b) The sliced image of O^- ions at the electron incident energy of 8.3eV. (c) The angular distribution plot of O^- with the kinetic energies of 0.4–0.7 eV [obtained from the sliced image (b)]. (d) The sliced image of O^- ions at the electron incident energy of 7.3 eV. The electron incident direction is from left to right. In the images, the ion intensities are normalized with their respective highest values.

Limitation

- Diamond turning and molding
- Printing
- Expanding and shrinkage
- Gravity

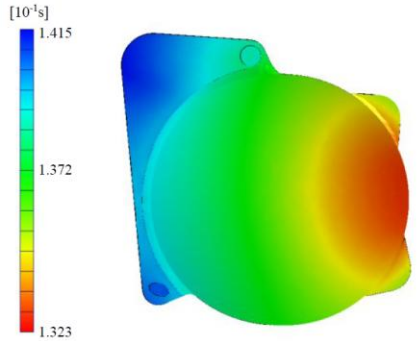

Figure 6. Simulation of the melt front time.

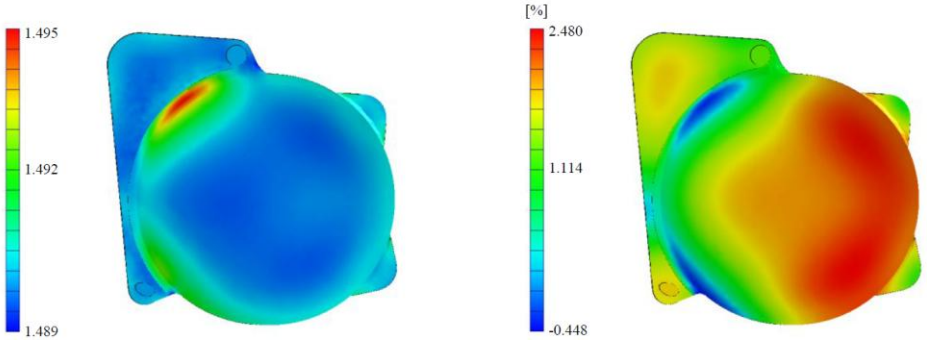

Figure 7. Simulation of the distribution of the refractive index (left) and the volumetric shrinkage (right).

NASA
THIS BALL OF WATER IS FLOATING IN
THE INTERNATIONAL SPACE STATION

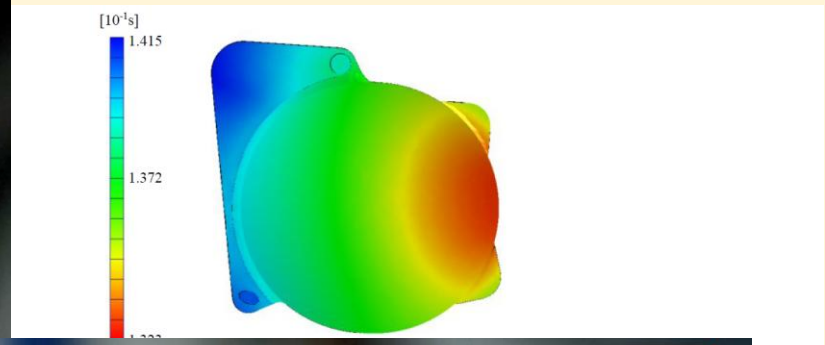
[10⁻¹s]
1.415
1.372

NASA
BUT THIS TIME
THEY ARE
TESTING
A NEW 4K
CAMERA
CNN